

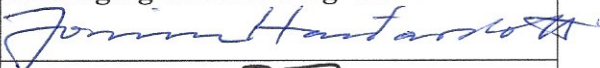
The ICRA atmospheric reanalysis project for Iceland

Nikolai Nawri
Bolli Pálmason
Guðrún Nína Petersen
Halldór Björnsson
Sigurður Þorsteinsson

The ICRA atmospheric reanalysis project for Iceland

Nikolai Nawri, Icelandic Met Office
Bolli Pálmason, Icelandic Met Office
Guðrún Nína Petersen, Icelandic Met Office
Halldór Björnsson, Icelandic Met Office
Sigurður Þorsteinsson, Icelandic Met Office

Keypage

Report no.: VÍ 2017-005	Date.: May 2017	ISSN: 1670-8261	Public <input checked="" type="checkbox"/> Restricted <input type="checkbox"/> Provision:
Report title / including subtitle The ICRA atmospheric reanalysis project for Iceland		No. of copies: 8 Pages: 37	
		Managing director: Jórunn Harðardóttir	
Author(s): Nikolai Nawri, Bolli Pálmason, Guðrún Nína Petersen, Halldór Björnsson & Sigurður Þorsteinsson		Project manager: Halldór Björnsson	
		Project number: 5818-0-0001	
Project phase:		Case number: 2017-125	
Report contracted for:			
In cooperation with:			
Summary: This report describes the technical aspects of the ICRA reanalysis project for Iceland, which was initiated by the Icelandic Meteorological Office in the autumn of 2015, using the HARMONIE-AROME mesoscale numerical weather prediction model. It also describes, for the first time, the surface energy balance over the entire land area of Iceland, establishing the relative importance of radiation and heat fluxes, their spatial variability, and changes on diurnal and seasonal time-scales. It is then shown how the temporal and spatial variability of energy fluxes is related to the variability of different boundary layer properties, such as the diurnal temperature range, diurnal shifts in the horizontal wind field, and the vertical gradients of temperature and wind speed. Furthermore, a number of statistics are discussed, such as frost and growth days, or of precipitation events with specific durations and intensities.			
Keywords: HARMONIE-AROME numerical weather prediction model Reanalysis Atmospheric boundary layer Iceland		Managing director's signature: 	
		Project manager's signature: 	
		Reviewed by: SG	

Contents

1	Introduction	7
2	Model setup and archived data	7
3	Air temperature biases over snow surfaces	14
4	Energy fluxes at the surface	14
5	Boundary layer properties	22
6	Precipitation	29
7	Conclusions	36
	References	36

List of Figures

1	Updated ECOCLIMAP-II database for Iceland.....	10
2	HARMONIE-AROME model dominant surface type.....	10
3	HARMONIE-AROME model terrain elevation.....	11
4	Excerpt from the sms/config_exp.h model configuration file	13
5	Evaluation of simulated 2-m air temperature	15
6	Total horizontal cloud cover	16
7	Snow water equivalent	17
8	Average daily sunshine hours.....	18
9	Mean monthly downward diffuse shortwave radiation flux at the surface.....	19
10	Mean monthly net downward longwave radiation flux at the surface.....	19
11	Mean monthly sensible heat flux from the ground	20
12	Mean monthly latent heat flux from the ground.....	20
13	Mean monthly daytime energy balance at the surface.....	21
14	Mean monthly nighttime energy balance at the surface.....	21
15	Mean monthly diurnal temperature range	23
16	Mean monthly vertical temperature gradient	23
17	Mean monthly height of the lifted condensation level.....	24
18	Monthly occurrence of frost days	25
19	Monthly growing degree days	26
20	Prevailing 10-m wind conditions during the day.....	27
21	Prevailing 10-m wind conditions during the night	27
22	Mean monthly vertical gradient of wind speed.....	28
23	Mean monthly wind power density at 50 m above ground	28
24	Precipitation biases relative to original and wind-loss corrected measurements	29
25	Percentage number of days with under-predicted precipitation amounts	30
26	Monthly accumulation of total precipitation.....	31
27	Difference in net precipitation between day and night	32
28	Occurrence of precipitation events lasting up to 6 hours	33
29	Occurrence of precipitation events lasting more than 6 and up to 12 hours.....	33
30	Average intensity of precipitation events lasting up to 6 hours.....	34
31	Occurrence of precipitation events with total accumulation of up to 30 mm	34
32	Mean monthly accumulation of liquid water on the ground	35

1 Introduction

In the autumn of 2015, the Icelandic Meteorological Office (IMO) initiated an ongoing atmospheric reanalysis project for Iceland (ICRA), using the HARMONIE-AROME mesoscale numerical weather prediction model, running on a supercomputer at the European Centre for Medium Range Weather Forecasts (ECMWF). This was preceded by an extensive test period, starting in the spring of 2013, during which the model was adapted and optimised for the Icelandic domain.

Initial and boundary conditions for the model simulations were provided by the ERA-Interim reanalysis, which goes back to 1979, the year when passive microwave data from satellites became available. ICRA starts on 1 September 1979 (the beginning of the hydrological year), and currently ends on 31 December 2016. This provides data for either 37 complete calendar years (January 1980 through December 2016) or 37 complete hydrological years (September 1979 through August 2016). For the whole period, hourly fields with a horizontal grid-point spacing of 2.5 km have been archived for all variables that are commonly used in studies of the atmospheric boundary layer (see Section 2 for a complete list).

This report describes the precise details of the model setup and forecast strategy, followed by a brief discussion of some of the information that can be obtained from the new dataset, either directly, or through derived parameters. Thereby, the emphasis is on those variables whose temporal and spatial variability highlights the impact of forcing mechanisms that are the result of seasonal changes in insolation, as well as geographical differences.

This report is organised as follows. Section 2 gives a detailed description of the setup of the HARMONIE-AROME model for ICRA, as well as a complete list of all archived variables. Section 3 briefly discusses 2-m air temperature biases that exist over snow-covered ground, and describes a methodology of reducing these biases by projecting temperature values down from the lowest two model levels. The seasonal cycle of radiation and heat fluxes is described in Section 4, followed by a description of the impact of these energy fluxes on different boundary layer properties in Section 5. Monthly accumulation of precipitation, as well as changes throughout the year in the average duration and intensity of individual precipitation events, is discussed in Section 6.

2 Model setup and archived data

The equations and parameterisations that constitute the core of the HARMONIE-AROME model are described by Brousseau et al. (2011), Seity et al. (2011), and Bengtsson et al. (2017). The specific model version used for ICRA is 38h1.2. The simulations were done on the cca supercomputer at ECMWF. To make the reanalysis data compatible with the IMO operational runs, for the purpose of establishing a background statistics, the model was run in numerical weather prediction (rather than climate) mode.

HARMONIE-AROME uses a terrain-following sigma coordinate system, where model levels are defined as iso-surfaces of pressure, scaled by the surface pressure. As such, model level heights vary in time and space. For the standard 65 vertical model levels, used for both ICRA and the IMO operational runs, the ranges of the actual (geometrical) heights above ground of the lowest 15 model levels in January and July are given in Table 1.

The chosen dynamic core of the model is non-hydrostatic. Radiation, turbulence, convection, and microphysics (clouds and precipitation) are determined by the AROME upper air physics scheme. Surface and soil processes are described by version 7.2 of the external single-layer coupled surface scheme SURFEX, consisting of special components for four different surface types: natural land surfaces (including vegetation, bare soils, rocks, and permanent snow), town (including buildings, roads, gardens, and parks), inland water (including lakes and rivers), and ocean (including also sea ice) (Le Moigne, 2009). SURFEX uses input from the lowest level of the atmospheric model, together with static fields describing the model terrain, to calculate radiative surface properties, as well as surface fluxes of momentum, sensible and latent heat, aerosols, CO₂, and various other chemical species. These properties are then used as lower boundary conditions for the upper air dynamical model and physics scheme, and to calculate fixed-height atmospheric variables near the surface that are not located on model levels, such as 2-m air temperature, and 10-m horizontal wind.

Initial and boundary conditions for ICRA were provided by ERA-Interim reanalyses, with a boundary data interval of 6 hours (Andersson & Thépaut, 2008; Bechtold et al., 2008). The lateral boundaries of the model have a relaxation zone of 10 grid points, wherein the coarse-resolution outer data from the host model is blended with the high-resolution data within the

Table 1. Heights above ground [m] of the lowest 15 model levels in January and July. Averages and extreme values are determined over the land area of Iceland, excluding the oceans.

	January			July		
	Min.	Ave.	Max.	Min.	Ave.	Max.
L51	476	510	535	502	525	547
L52	423	453	476	446	467	486
L53	375	402	421	395	414	431
L54	330	354	371	348	364	380
L55	289	310	326	305	319	333
L56	251	270	283	265	278	290
L57	216	233	244	229	240	250
L58	184	199	208	195	205	214
L59	155	167	175	164	172	180
L60	127	137	144	135	142	148
L61	102	110	115	108	113	119
L62	78	84	88	82	87	91
L63	55	59	62	58	61	64
L64	33	35	37	35	36	38
L65	11	12	13	11	12	13

dependent model domain. At the upper boundary, defined as the 10-hPa isobaric surface, vertical velocity is set to zero.

The model is run in upper-air and surface data assimilation mode. The atmospheric analysis is handled such that initial and boundary conditions, for each forecast run, are combined with coinciding output from the previous run (blending mode). Gridded surface analyses for 2-m air temperature and relative humidity, sea surface temperature, and snow water equivalent are prepared by the spatial interpolation tool CANARI.

As discussed in Nawri (2014), spin-up effects during the first 6 hours of each forecast cycle result in discontinuities between the initial and boundary conditions, and the internal model climate. Therefore, for ICRA, only forecast hours 6 to 12 are being used to concatenate longer time-series from the 6-hourly individual forecast runs. This eliminates all spin-up effects.

To prevent an unrealistic accumulation of snow in the elevated interior of the island, the model is run continuously only for individual hydrological years, which are defined to begin on 1 September. The spin-up period for each annual simulation begins with a cold-start on 20 August at 0 UTC, for which all snow cover is removed from the land area outside the glaciers. As in the operational runs, glaciers are simulated by placing $10,000 \text{ kg m}^{-2}$ (10 m of snow water equivalent) on top of the permanent snow regions, as defined by the model physiography. This is done to give glaciers realistic radiative and thermodynamic properties, including the ability to melt.

The ICELAND domain was defined in the `scr/HARMONIE-AROME_domains.pm` script such that it has 300×240 horizontal grid points, centred at (19.0°W , 64.7°N), and a horizontal grid-point spacing of 2.5 km in both directions. In conjunction with this spatial resolution, the model time-step was set to the default of 45 seconds. Iceland is the only landmass inside the model domain. This model domain is consistent with that of the operational forecast runs until September 2015. Since then, the operational domain has been increased in size.

Nawri (2014) discussed some of the problems that existed with the default model physiography for Iceland, based on ECOCLIMAP-II, which had not been updated from ECOCLIMAP-I for Iceland. As described in Palmason et al. (2016), these geographical errors have since been corrected by compiling an updated physiography specifically for Iceland (see Figure 1). However, as of the time of publication of this report, the updated version has not been incorporated into the official ECOCLIMAP-II database. The main problem with the old physiography is an overrepresentation of wet and vegetated regions. Therefore, based on local measurements and MODIS satellite data, vegetation fraction and leaf area index were adjusted, which resulted in more realistic surface roughness lengths and surface albedo. Soil types and depths were completely redefined across the island. Also corrected were some errors associated with terrain elevation. The resulting dominant surface types (those which contribute to more than 50% of the surface area within each grid box) and model terrain elevation are shown in Figures 2 and 3, respectively.

Aside from the comprehensive update of the physiography, only few changes were made from the default model setup.

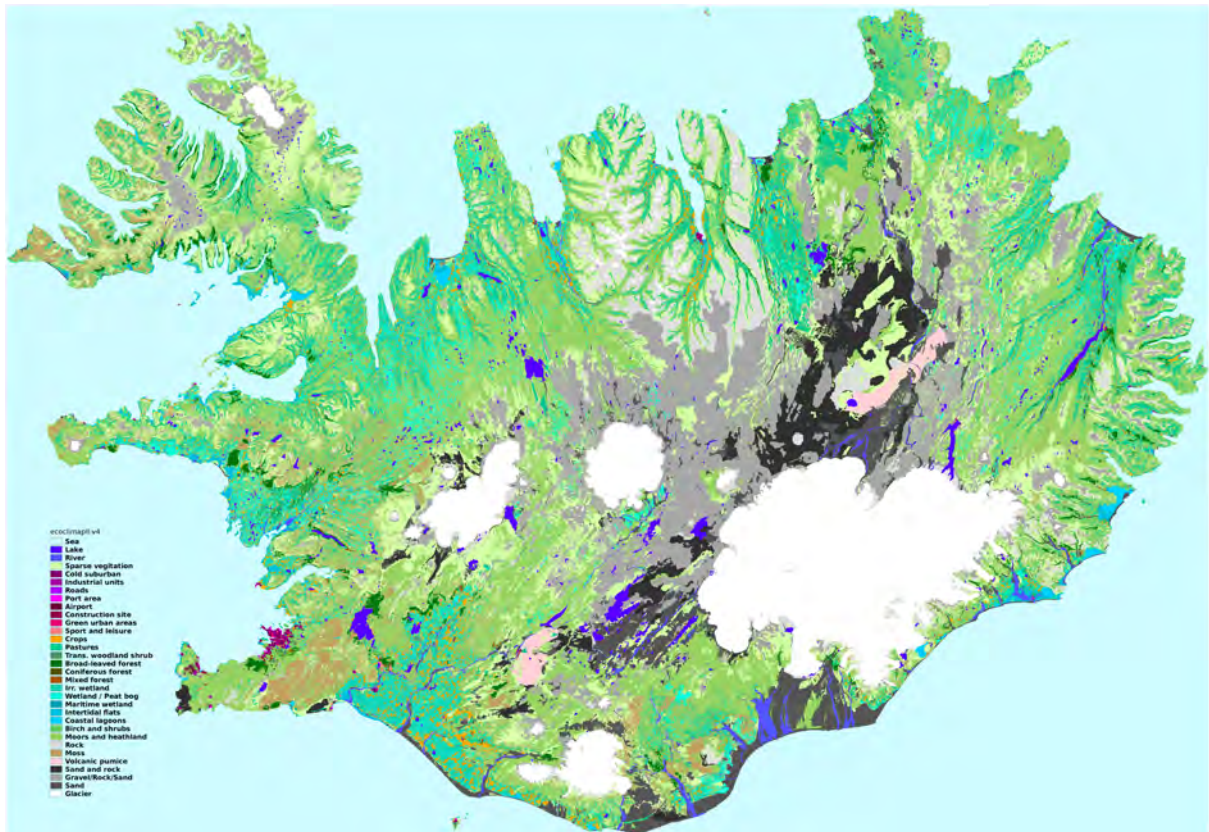


Figure 1. Updated ECOCLIMAP-II database for Iceland.

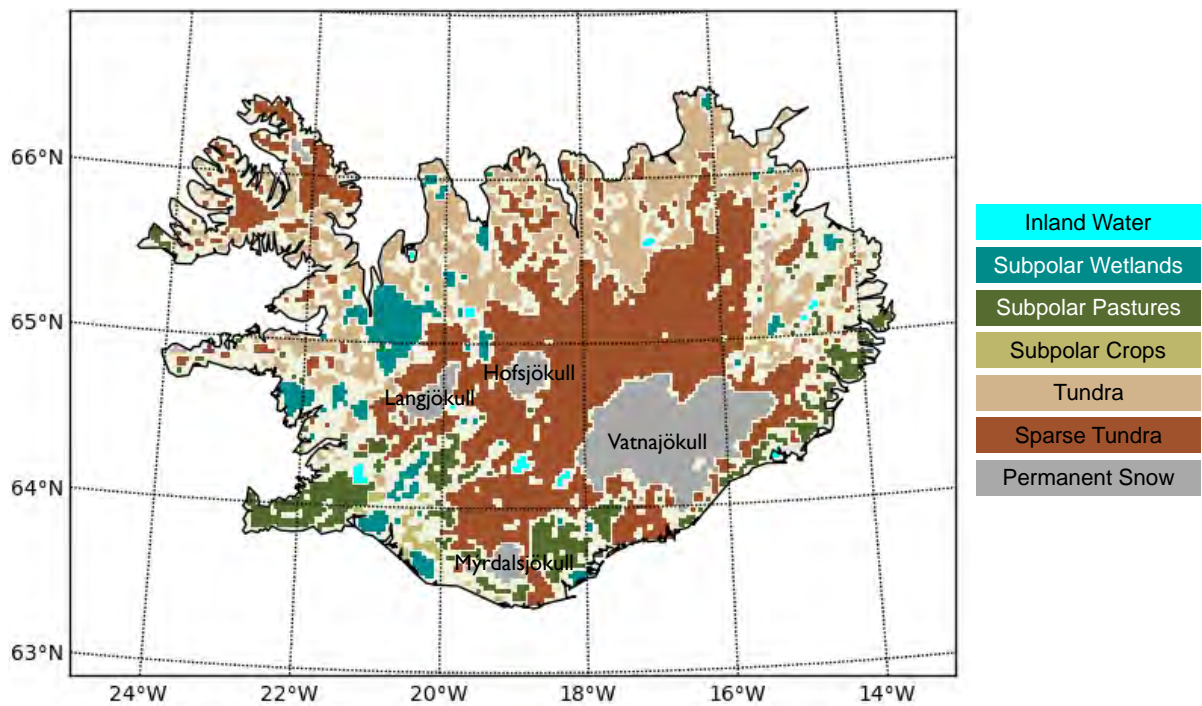


Figure 2. HARMONIE-AROME model dominant surface type.

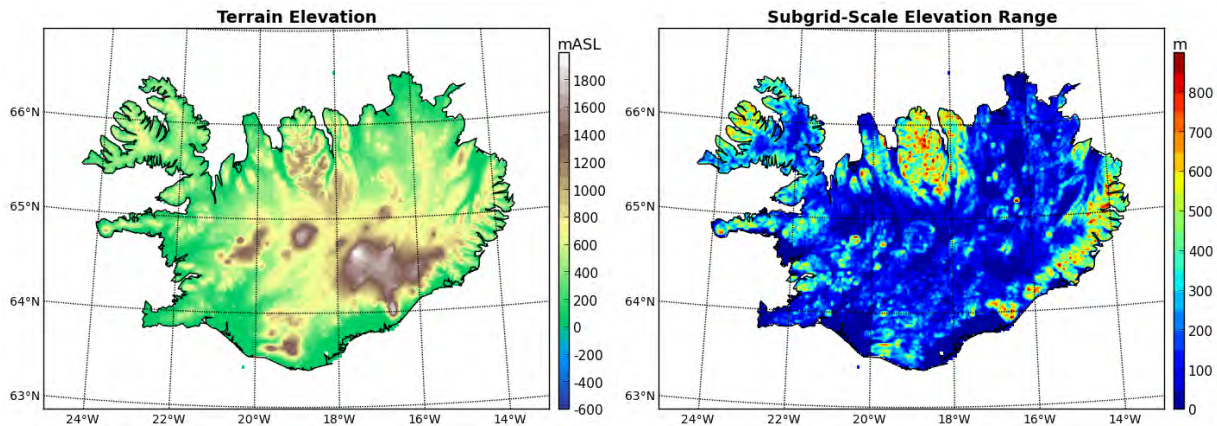


Figure 3. HARMONIE-AROME model terrain elevation.

In the namelist `nam/HARMONIE-AROME_namelists.pm`, the logical switch `LOCND2` was set to `FALSE`. This turns off a new mixed cloud option with a separate ice-phase representation, which was introduced first in model cycle 38h1.2. It allows the possibility for snow and mixed-phase precipitation to affect radiation fluxes. However, aside from technical problems (slow computational speed and serious stability issues), the new cloud scheme led to significantly reduced snowfall over Iceland, and an unrealistically low snow cover on the ground, compared with MODIS satellite images.

In the namelist `nam/surfex_namelists.pm`, the logical switch `LSWEMAX` was set to `FALSE`. This was necessary to prevent the capping of snow depth on the glaciers. As mentioned above, permanent snow cover, in the current setup of HARMONIE-AROME for IMO applications, is simulated by a thick layer of regular (variable) snow on the ground.

In the default version of the script `scr/MARS_get_bd`, the horizontal resolution of boundary data is increased from 0.50 degrees in latitude and longitude to 0.25 degrees, for simulation periods on or after 1 February 2006, 06 UTC. An additional increase in resolution to 0.15 degrees is done for simulation periods on or after 26 January 2010, 06 UTC. For ICRA (not for the IMO operational runs), to prevent inconsistencies throughout the simulated period, the horizontal resolution of boundary data was kept fixed at 0.50 degrees.

In the code `src/surfex/SURFEX/ini_surf_csts.F90`, surface roughness length of momentum over snow, `XZ0SN`, was increased from 0.001 to 0.005, to reduce positive biases in wind speed over snow-covered areas. Other physical parameters that crucially influence radiation and heat fluxes at the surface, and for which default values were used, are surface roughness length of heat over snow, `XZ0HSN = 0.0001`; emissivity of snow, `XEMISSN = 1.0`; emissivity of water, `XEMISWAT = 0.98`; minimum albedo of snow surfaces, `XANSMIN = 0.50`; maximum albedo of snow surfaces, `XANSMAX = 0.85`; and global albedo of water, `XALBWAT = 0.135`.

In addition to the description given here, see Figure 4 for an excerpt from the `sms/config_exp.h` model configuration file, which provides several other relevant details about the model setup.

The simulated variables (horizontal fields) that were archived for each hourly time-step are:

- Fields on the lowest 15 model levels: temperature, specific humidity, horizontal wind components, turbulent kinetic energy
- Fields on constant pressure levels at 1000, 925, 850, and 500 hPa: geopotential, temperature, relative humidity, horizontal wind components
- Fields at 500 and 1000 m above ground: temperature, relative humidity, horizontal wind components
- Surface and boundary layer fields: air pressure and temperature at ground level, mean sea level pressure, 2-m air temperature, 2-m specific and relative humidity, 10-m horizontal wind components, snow depth on the ground (liquid water equivalent), atmospheric mixed layer depth, total cloud cover, low/medium/high cloud cover, convective cloud cover, total latent heat flux from the ground
- Surface layer accumulated fields: short- and longwave downward radiation flux, short- and longwave net downward radiation flux, direct solar radiation flux, upward sensible heat flux, separate upward latent heat fluxes for evaporation and sublimation, masses of water evaporation and snow sublimation, mass of rainwater, mass of snow, mass of mixed-phase precipitation (referred to in the model as graupel)

```

:
:
RUNNING_MODE=research
:
:
SIMULATION_TYPE=nwp
**** Model geometry ****
DOMAIN=ICELAND
VLEV=65
LL=${LL-12}
**** High level forecast options ****
DYNAMICS="nh"
PHYSICS="arome"
SURFACE="surfex"
DFI="none"
LSPBDC=no
LGRADSP=yes
LUNBC=yes
**** Highlighted physics switches ****
CISBA="3-L"
CROUGH="NONE"
**** Assimilation ****
ANAATMO=blending
ANASURF=CANARI_OI_MAIN

ANASURF_INLINE="yes"
ANASURF_MODE="before"

INCV="1,1,1,1"
INCO="1,1,0"
MAKEODB2=no
SST=BOUNDARY

LSMIXBC=no
["$ANAATM" = 3DVAR] && LSMIXBC=yes
JB_INTERPOL=no
FCINT=06

:
:
**** DFI setting ****
TAUS=5400
TSPAN=5400
**** Nesting ****
HOST_MODEL="ifs"

HOST_SURFEX="no"
SURFEX_INPUT_FORMAT=lfi
NBDMAX=12
BDLIB=ECMWF

:
:
BDSTRATEGY=era

BDINT=6
SURFEX_PREP="yes"

:
:
**** Physiography input for SURFEX ****
ECOCLIMAP_VERSION=2.2

SOIL_TEXTURE_VERSION=HWSD_v2

:
:

```

```

:
:
Research or operational mode (research|operational)
operational implies that
- Not STAGE is done for MARS requests
- No assimilation is done if no obserations are found by Bator
Type of simulation (nwp|climate)

See definitions in scr/HARMONIE-AROME_domains.pm
Vertical level definition.
Forecast length [h]

Hydrostatic or non-hydrostatic dynamics (h|nh)
Main model physics flag (arome|alaro)
Surface flag (old_surface|surfex)
Digital filter initialization (idfi|fdfi|none)
Spectral boundary contions option off(no) | on(yes)
Apply Wedi/Hortal vorticity dealiasing
Apply upper nested boundary condition

Type of ISBA scheme in SURFEX. Options: "3-L" and "2-L"
SSO scheme used in SURFEX "NONE"|"Z01D"|"BE04"

Atmospheric analysis (3DVAR|4DVAR|blending|none)
Surface analysis (CANARI|CANARI_OI_MAIN| CANARI_EKF_SURFEX|none)
CANARI: Old style CANARI
CANARI_OI_MAIN: CANARI + SURFEX OI
Calls SODA interface from inside CANARI if set to yes (experimental)
When ANASURF should be done
before: Before ANAATMO
Active EKF control variables. 1=WG2 2=WG1 3=TG2 4=TG1
Active EKF observation types (element 1=T2m, 2=RH2m, 3=soil moisture)
Conversion of ODB-1 to ODB-2 using odb_migrator
Which SST fields to be used in surface analysis
BOUNDARY: SST interpolated from the boundary file
Spectral mixing of LBC0 file before assimilation

Interpolation of structure functions to your domain
Assimilation cycle interval [h]

:
:

cut-off frequency in second
7200s or 5400s

Host model (ifs|hir|ald|ala|aro)
ifs: ecmwf data
yes if the host model is run with SURFEX
Input format for host model run with surfex (lfi|fa)
Number of parallel interpolation tasks
Boundary experiment, set:
ECMWF to use MARS data

:
:

Which boundary strategy to follow
as defined in scr/Boundary_strategy.pl
analysis_only: Use only analyses as boundaries
era: As for analysis_only but using ERA interim data
Boundary interval in hours
Use offline surfex prep facility (Alt. gl + Fullpos + prep )

:
:

Version of ECOCLIMAP for surfex (1,2)
Available versions are 1.1-1.5,2.0-2.2
Soil texture input data FAO|HWSD_v2

:
:

```

Figure 4. Excerpt from the sms/config_exp.h model configuration file.

3 Air temperature biases over snow surfaces

Unfortunately, the negative 2-m air temperature biases over Iceland, that had been discussed by Nawri (2014) for HARMONIE-AROME cycle 37h1.2, are still present with cycle 38h1.2. They are largest over snow-covered terrain. Following the procedure introduced by Nawri (2014), to reduce these biases, 2-m temperatures over grid-points with snow cover greater than zero were recalculated by linear projection from the lowest two model levels.

Figure 5 shows a comparison between quality controlled station measurements and model data, where model values at each station location are given by inverse distance weighted averages from the four surrounding grid-points. Using vertically projected values over snow, temperature biases in winter (DJF) are reduced by about a factor of two, from around -1.30°C for the original SURFEX data to around -0.63°C for the recalculated values, with only small fluctuations throughout the day. In summer (JJA), biases are smaller than in winter, ranging between $0.3 - 0.5^{\circ}\text{C}$ over the course of the day, and are similar for the original SURFEX and recalculated model data. The only differences exist at a few station locations on elevated terrain, where snow cover persists during part of the summer months.

In the following discussion, due to the reduced biases, only the recalculated 2-m air temperature data will be used.

4 Energy fluxes at the surface

Radiation and heat fluxes at the Earth's surface strongly depend on cloud conditions, as well as the radiative and thermodynamic properties of the ground.

The mean monthly total cloud cover is shown in Figure 6. Its seasonal cycle and geographical variability is similar to that of low cloud cover, whereas mid- and high-level clouds have lower average extent, and a weaker spatial variability (not shown). The average horizontal concentration of the overall cloud cover is therefore dominated by low clouds, which are defined in HARMONIE-AROME as being situated below the 0.8 sigma coordinate level. Over low terrain, this level fluctuates around 800 hPa, or about 1,800 m above ground. The low-cloud cover in the model can therefore include genuine low clouds (such as stratus or stratocumulus), as well as the bases of vertically developed clouds (such as cumulus or nimbostratus). Referring forward to Section 6, it is clear that on a monthly basis there is no correlation between horizontal cloud cover and precipitation, which strongly depends on the vertical extent of clouds and, unlike the horizontal cloud cover, is closely linked to the orography.

Over the course of a year, radiative and thermodynamic surface properties vary in response to changes in the vegetation and snow cover. For Iceland, with relatively sparse vegetation throughout the year, the dominant impact is from variations in the snow cover. As shown in Figure 7, starting in late September, snow cover extent and thickness gradually build up until they reach maxima in April, followed by a period of rapid melt in May and June. By August, almost all snow outside the glaciers has disappeared.¹

¹As mentioned in Section 2, the remaining snow outside the glaciers is removed at the beginning of each hydrological year.

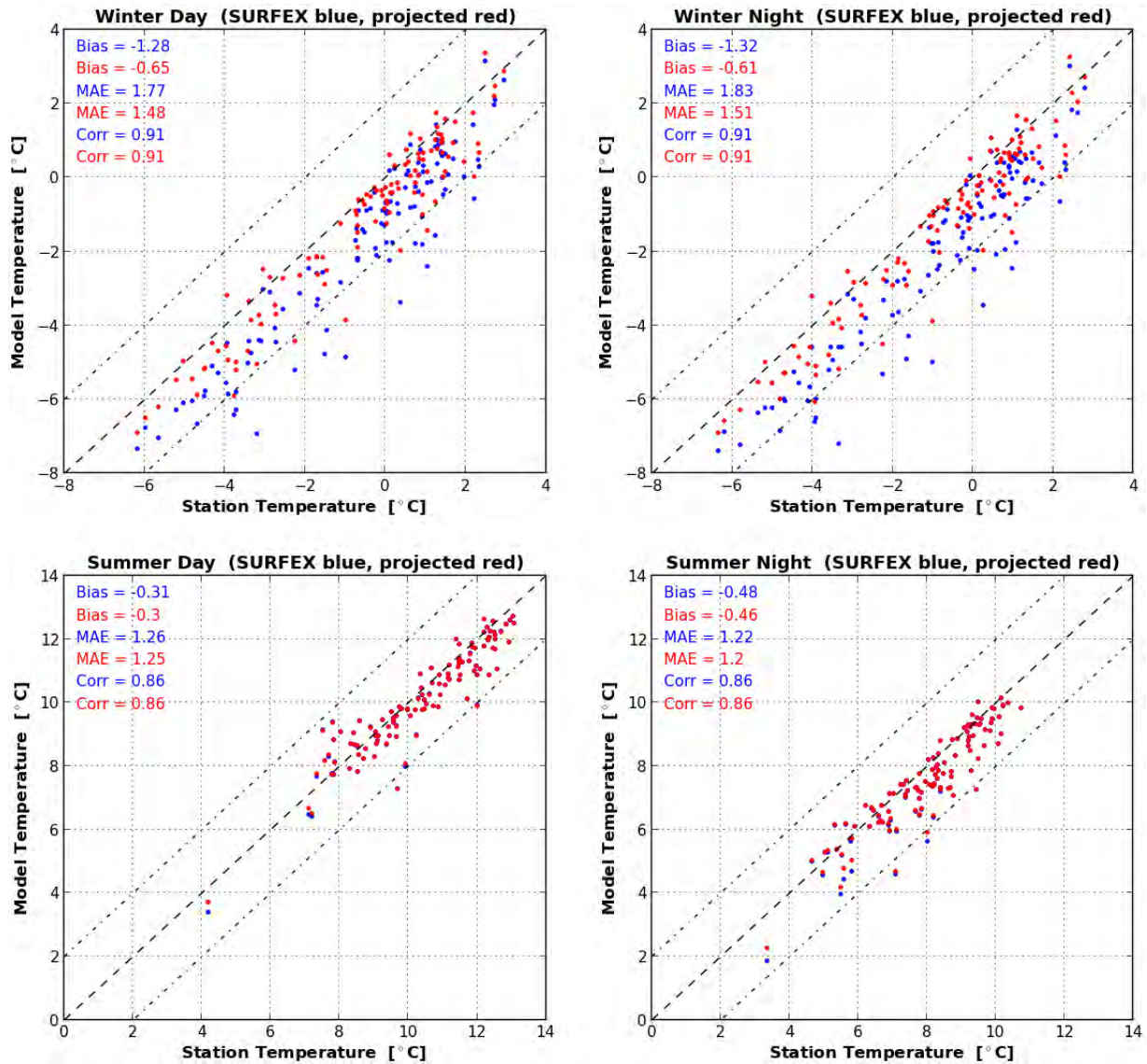


Figure 5. Mean errors (biases), mean absolute errors (MAE), and correlations between measured and simulated 2-m air temperature in winter (DJF) and summer (JJA). With solar noon between 13 – 14 UTC over Iceland, daytime hours are defined here as the period 08 – 19 UTC, and nighttime hours as the period 20 – 07 UTC. Original values from SURFEX are represented by the blue dots, values projected from the lowest model levels by the red dots.

Shortwave radiation received at the Earth’s surface is separated in the model into two components: direct and diffuse.

As a measure of physically significant direct shortwave radiation flux at the surface, average daily sunshine hours are shown in Figure 8. According to the World Meteorological Organization (WMO), sunshine hours are defined as the average period per day during which locally the direct shortwave radiation flux at the surface exceeds 120 W m^{-2} (WMO, 2012). This lower limit falls within the range of detection limits of different models of Campbell-Stokes sunshine recorders, although for current measurements of direct solar irradiance the use of a pyrheliometer

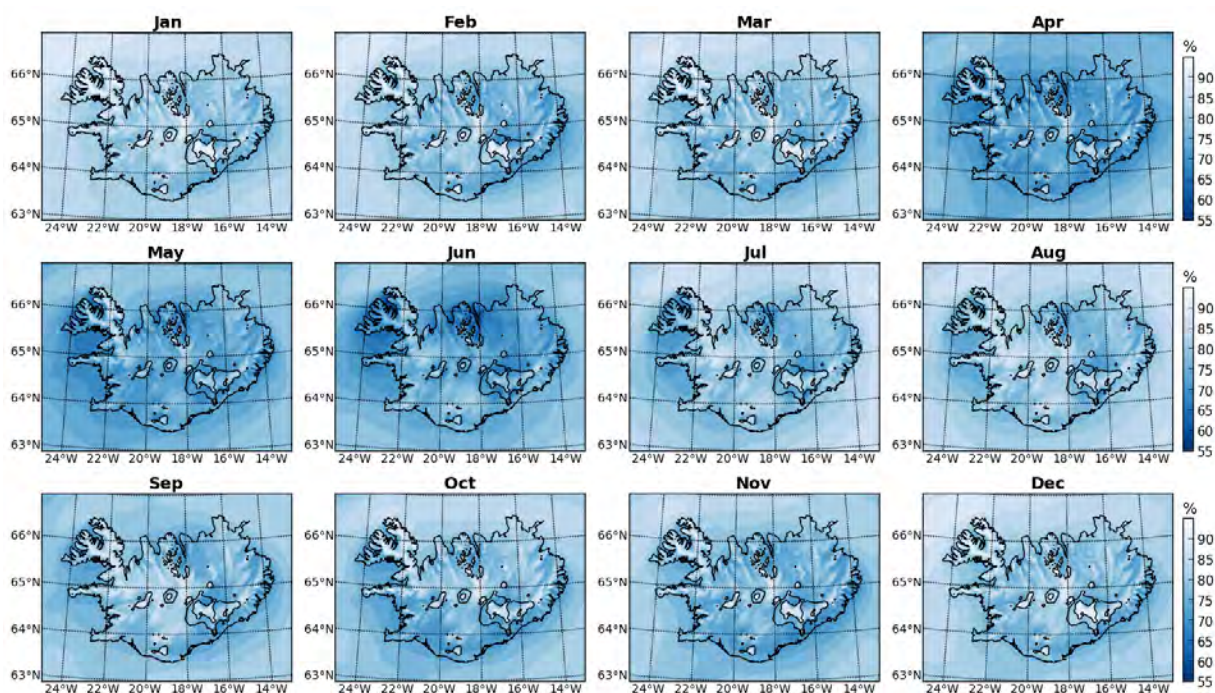


Figure 6. Total horizontal cloud cover in percent of each grid-box area.

is recommended. Sunlight with an intensity in excess of 120 W m^{-2} is considered “bright” in the sense of casting visible shadows, and “usable” for agricultural purposes in the sense of supporting plant growth. Comparing Figure 8 with Figure 6, it becomes clear that the spatial variability of sunshine hours is consistent with that of the average horizontal extent of the cloud cover.

While, within a given season, the amount of direct shortwave radiation at the surface primarily depends on cloud cover, the diffuse component of shortwave radiation is additionally affected by the presence of snow on the ground. In fact, as seen in Figure 9, in comparison with Figure 7, the high albedo of snow surfaces has a dominant effect, as it increases the reflection of incoming solar radiation, and therefore the atmospheric scatter of reflected radiation back to the ground. These multiple reflections also increase the total downwelling shortwave radiation flux (not shown). However, since atmospheric backscatter is weaker than reflection from snow-covered ground, the net shortwave radiation flux is reduced relative to snow-free ground (not shown).

The mean monthly net downward longwave radiation flux at the surface is shown in Figure 10. Its seasonal cycle depends on the relative heating and cooling of the atmosphere and the land surface. As the atmosphere heats up during the spring and summer months, the downward longwave radiation flux increases (see Figures 13 and 14). However, as the snow-free land area during that same period warms proportionally more, longwave radiation losses in these regions increase. The lowest longwave radiation losses occur along the edges of the glaciers in July and August, when a large amount of the incoming solar energy is used for melting, rather than increasing further the snow surface temperature.

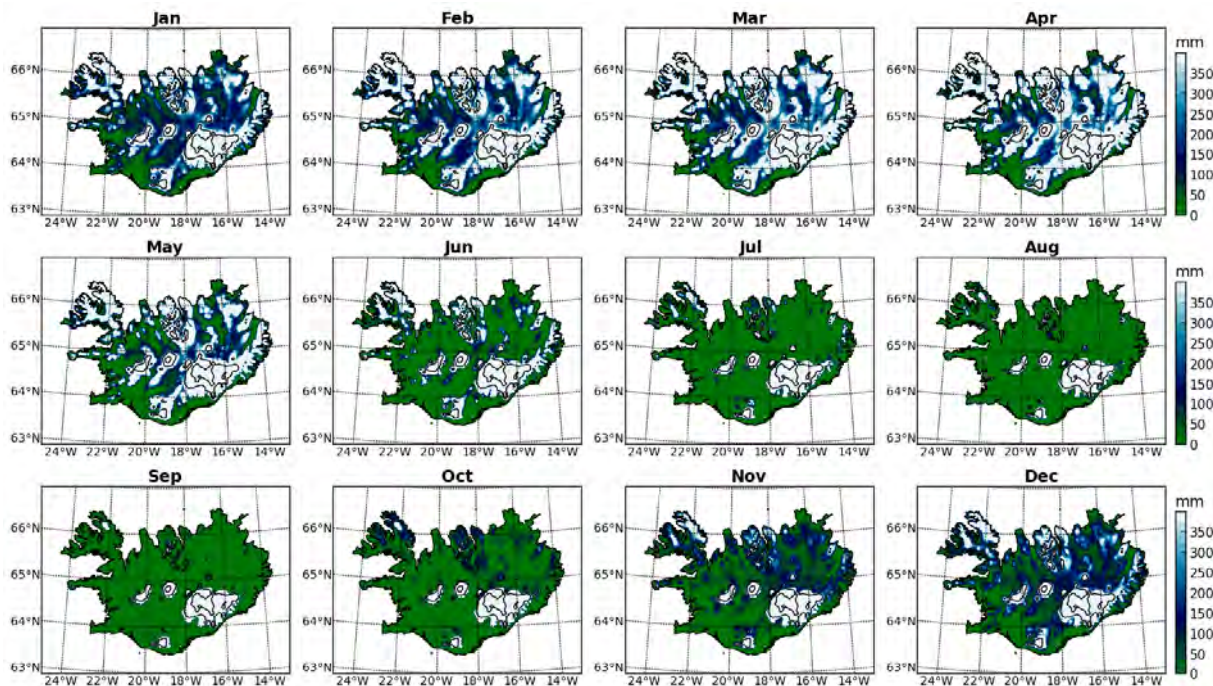


Figure 7. Snow cover on the ground, measured by the depth of an equivalent water column.

Sensible heat flux from the surface to the atmosphere is driven by the same radiative heating from the sun. Over snow-free ground, and especially over the sparsely vegetated interior highlands, there is therefore a similar seasonal cycle of sensible heat flux, with a similar spatial variability, as for longwave radiation losses (see Figure 11). The highest values occur in June over the extensive region of sand and dark volcanic rocks north of Vatnajökull. Over the ocean, sensible heat fluxes are positive, with the exception of the north and east coast during the summer months. This is consistent with the relatively low summertime sea surface temperatures (SSTs) in that region, found by Hanna et al. (2006) based on satellite data. The northeast to southwest gradient in SST around Iceland is maintained by the contrast between the East Iceland Current (a relatively cold and fresh branch of the East Greenland Current), which flows southward past the northeast coast of Iceland, and the Irminger Current (a relatively warm and saline branch of the North Atlantic Drift), which flows westward along the southwest coast.

Latent heat fluxes from the ground to the atmosphere additionally require the presence of water that is trapped near the surface, either in the soil or in the vegetation. To a lesser extent, sublimation from snow-covered ground also contributes to the overall latent heat flux. As shown in Figure 12, the largest latent heat fluxes occur in June and July over snow-free but wet (e.g., from recent snowmelt) or densely vegetated ground, especially in the southwest.

The mean monthly energy balance at the surface, averaged across the land area outside the glaciers, is shown in Figures 13 and 14, for day- and nighttime hours, respectively. Since solar noon in Iceland varies between 13 – 14 UTC over the course of the year, “day” is defined here as 10 – 17 UTC, and “night” as 22 – 05 UTC.

During the day, total (direct and diffuse) downwelling shortwave radiation increases from essentially zero in December to almost 500 W m^{-2} in May and June. The relative difference between

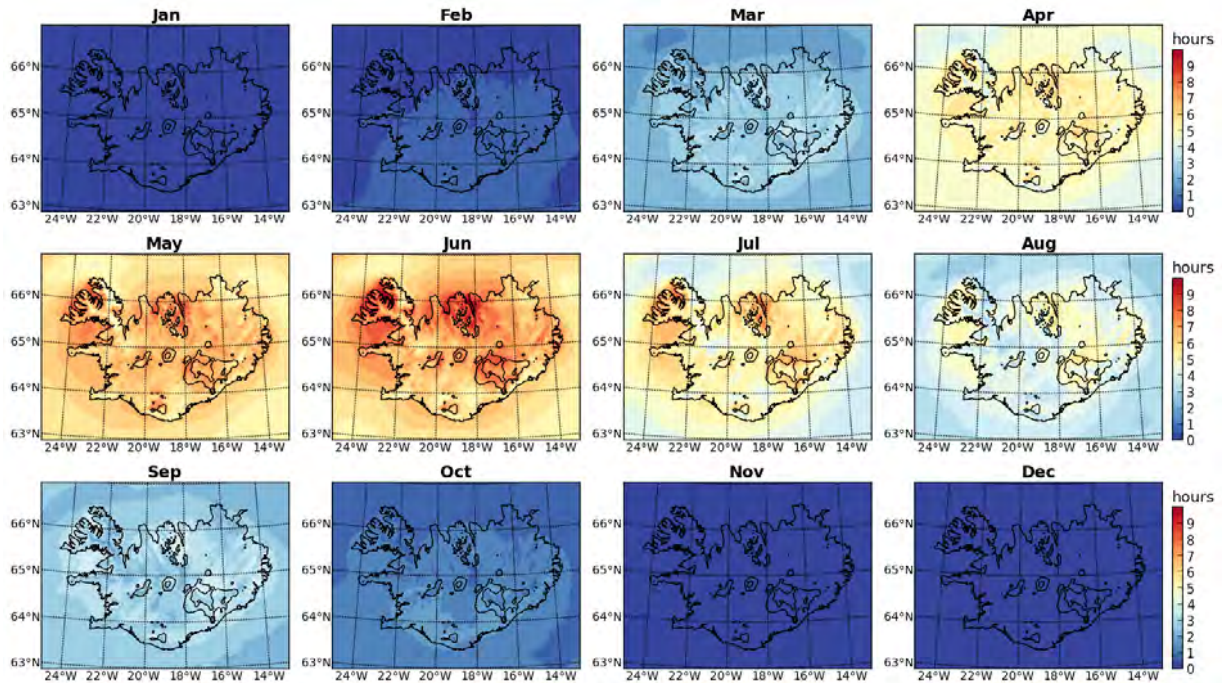


Figure 8. Average daily sunshine hours, with a direct shortwave radiation flux at the surface in excess of 120 W m^{-2} .

total and net downwelling shortwave radiation decreases from winter to summer, as the extent of snow cover is reduced, and the surface albedo decreases. Downwelling longwave radiation increases from 250 W m^{-2} in winter to just over 300 W m^{-2} in summer, while net longwave radiation losses increase from 30 W m^{-2} to 80 W m^{-2} . Between October and March, average sensible heat fluxes are directed from the atmosphere to the ground. During the other half of the year, sensible heat fluxes are reversed, reaching a maximum of 110 W m^{-2} in June and July. Average latent heat fluxes are essentially zero in December, and reach a maximum of just over 100 W m^{-2} in July. These individual energy fluxes combine to a generally positive net downward balance at the surface, with highest values of $70 - 80 \text{ W m}^{-2}$ in May and June, which are responsible for the rapid snowmelt during that period.

At night, the seasonal cycle of energy fluxes is driven primarily by downwelling longwave radiation, which is essentially unchanged from the daytime averages. Average sensible heat fluxes are directed from the atmosphere to the ground throughout the year and are largest during the winter months, reflecting the cooling of the land relative to the overlying air. Average latent heat fluxes are negligible throughout the year. The net downward energy balance at the surface is generally negative, with the highest losses for the ground occurring in late summer and early autumn.

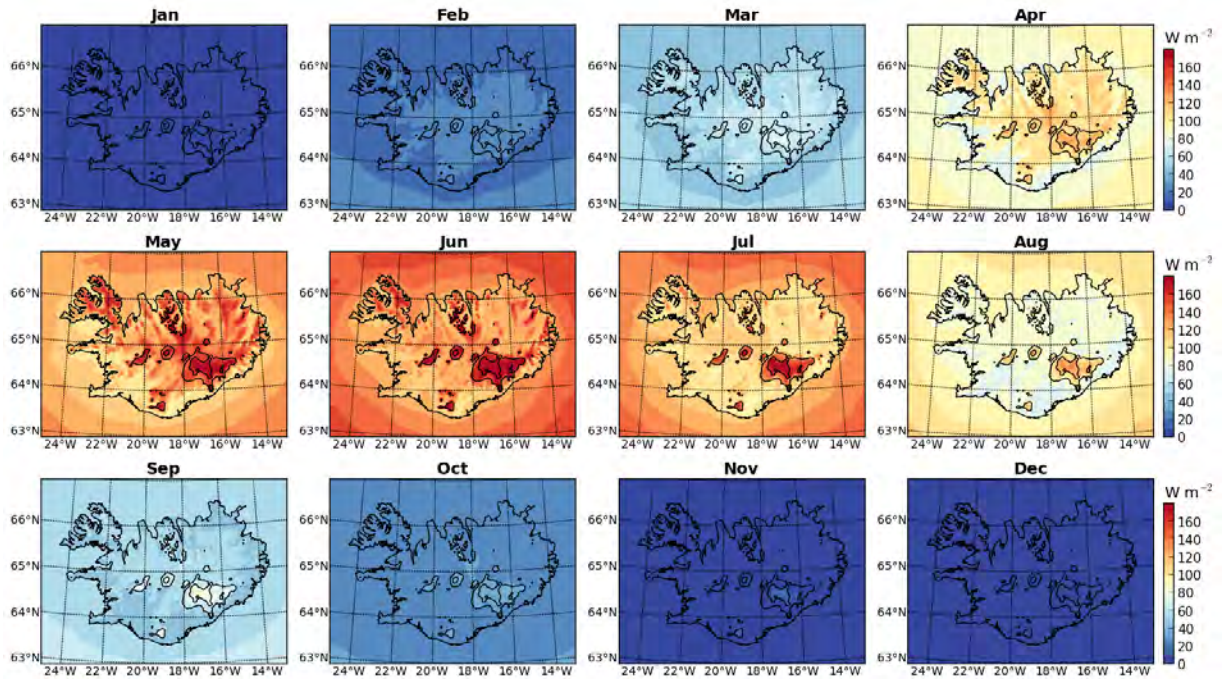


Figure 9. Mean monthly downward diffuse shortwave radiation flux at the surface.

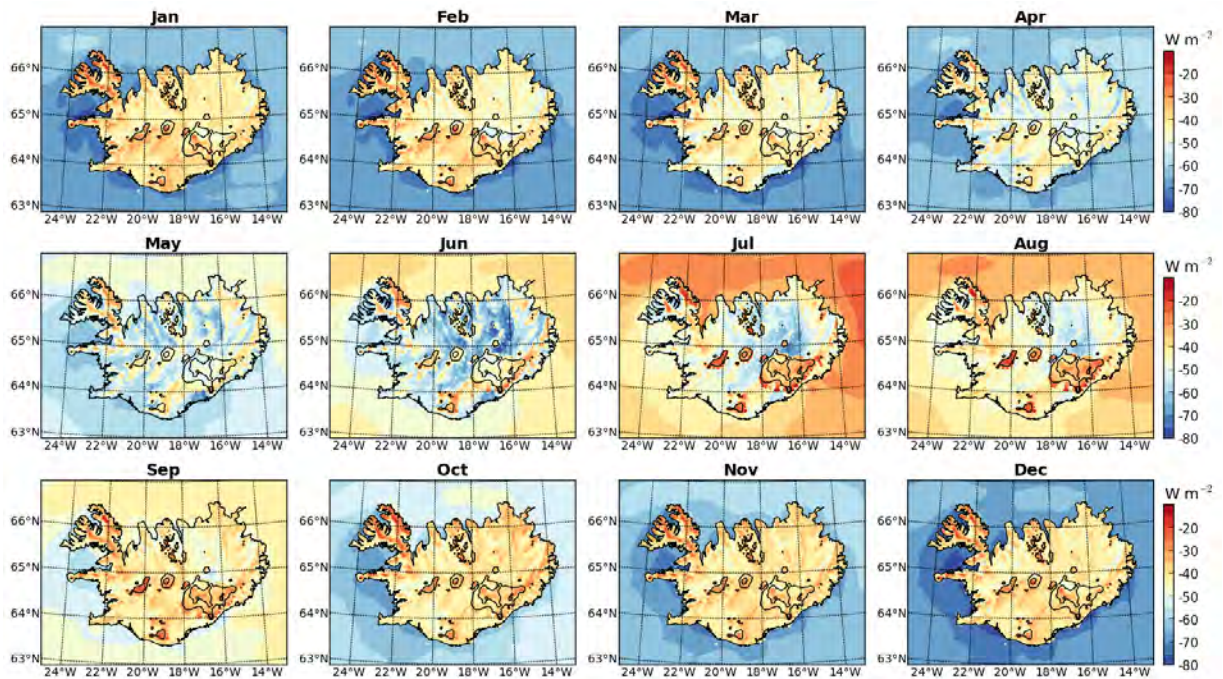


Figure 10. Mean monthly net downward longwave radiation flux at the surface.

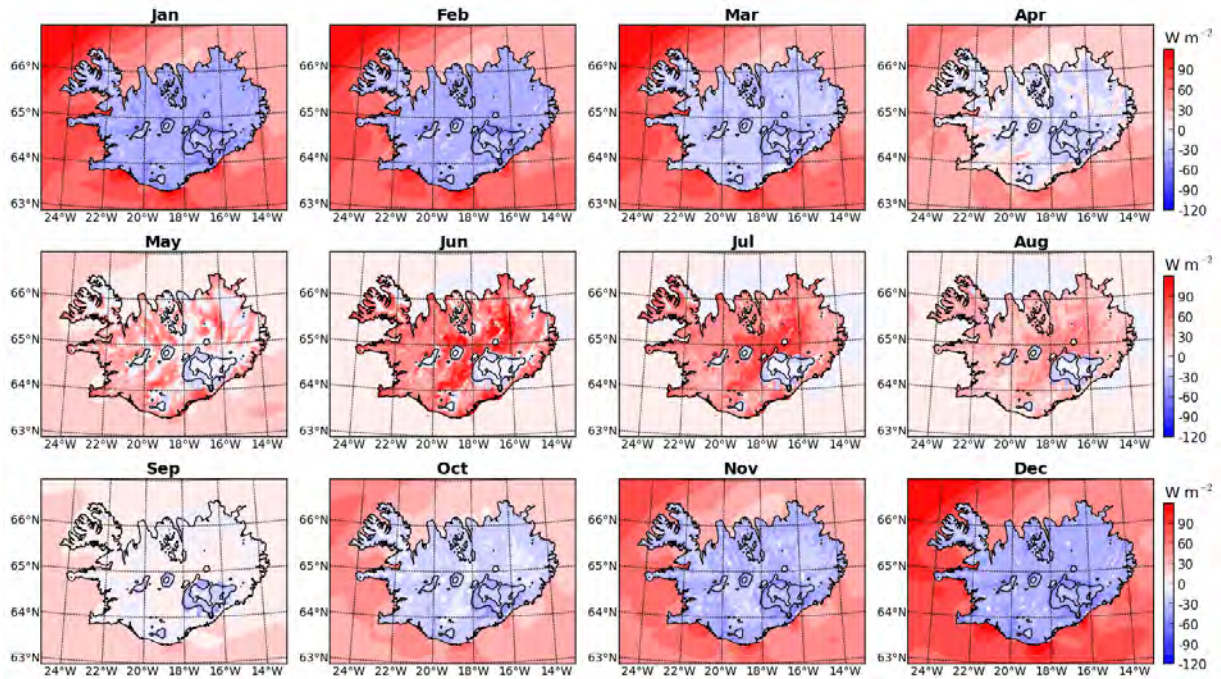


Figure 11. Mean monthly sensible heat flux from the ground to the atmosphere.

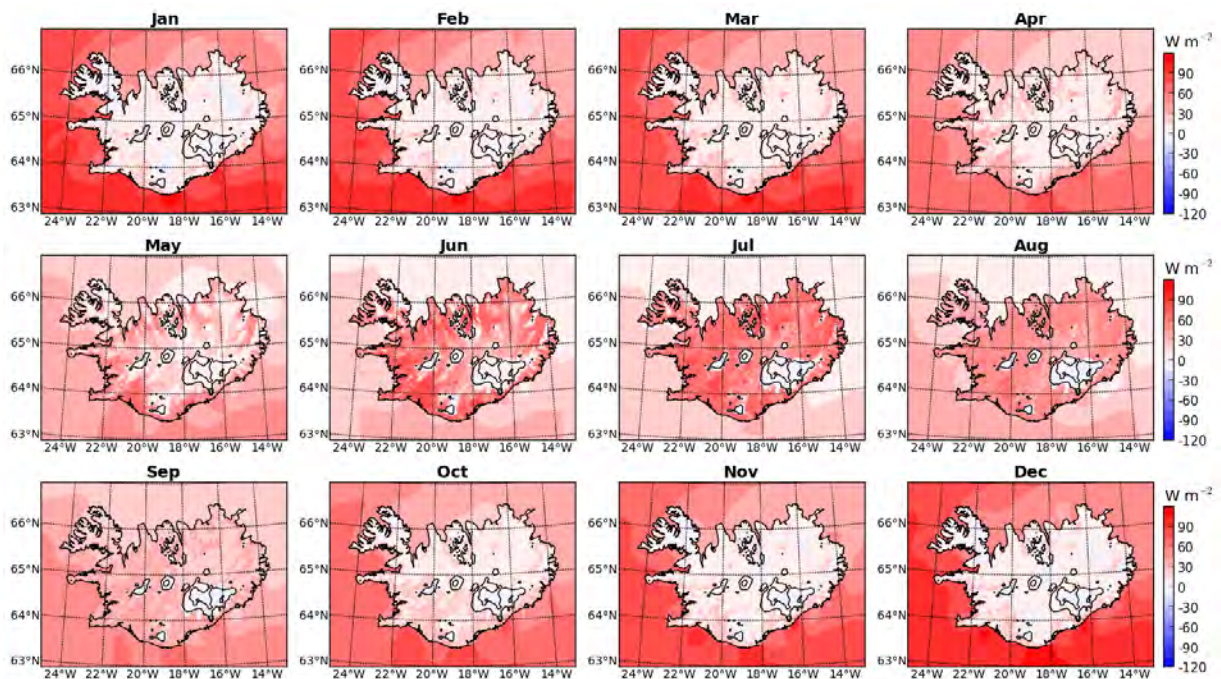


Figure 12. Mean monthly latent heat flux from the ground to the atmosphere.

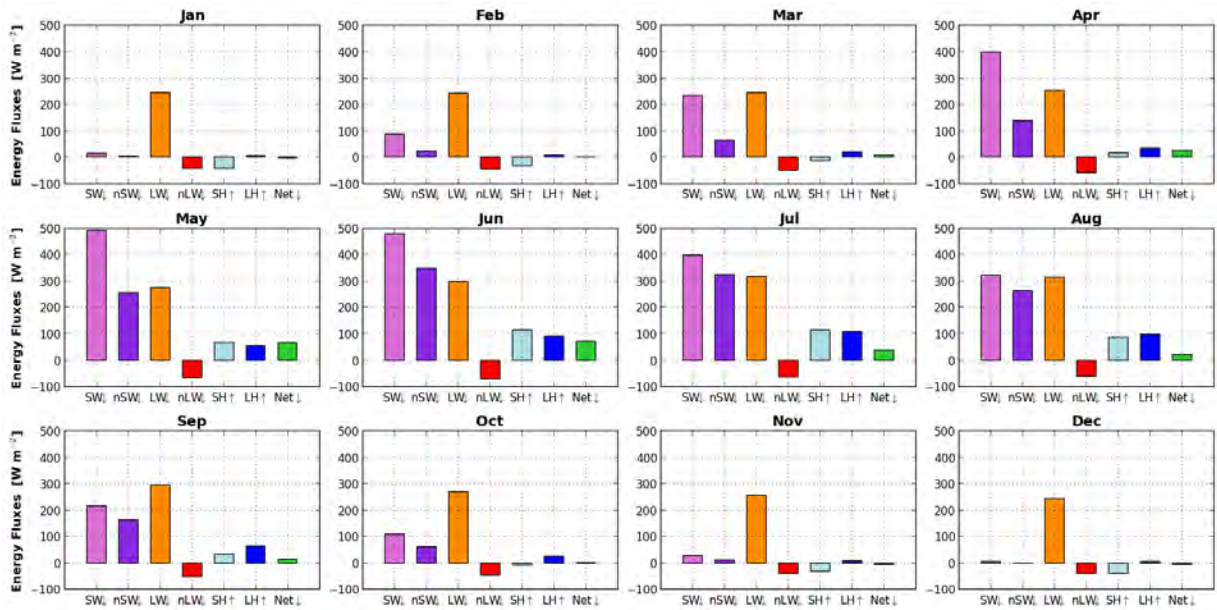


Figure 13. Mean monthly energy balance at the surface during the day (10 – 17 UTC), averaged across the land area outside the glaciers. The individual energy fluxes are total downward shortwave radiation, net downward shortwave radiation, total downward longwave radiation, net downward longwave radiation, upward sensible and latent heat flux, as well as the net downward flux.

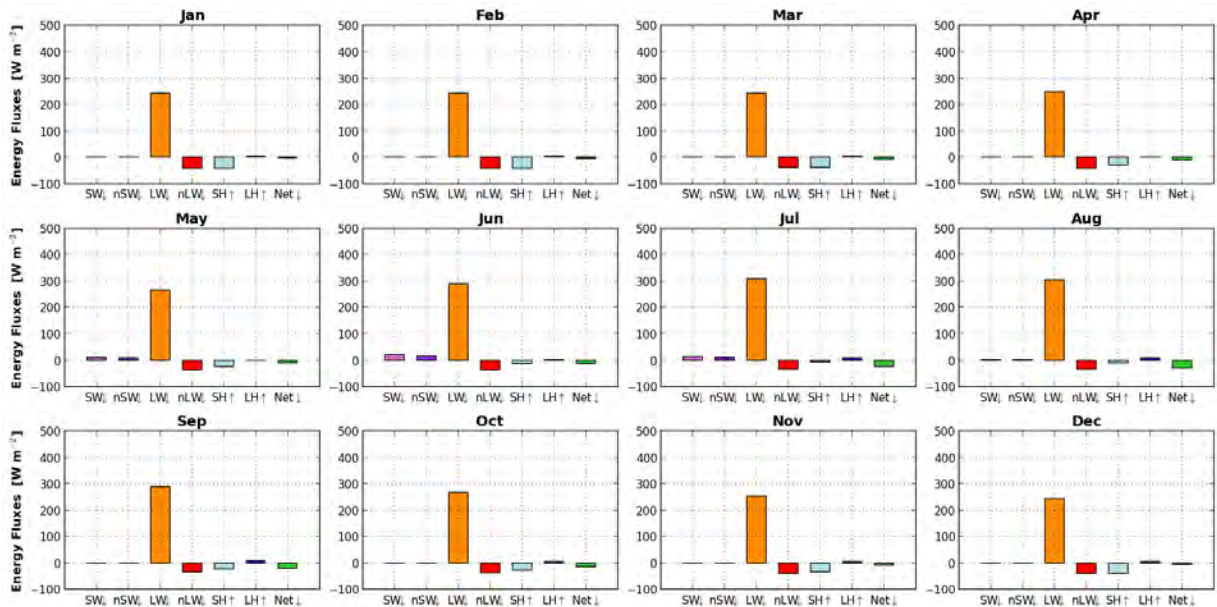


Figure 14. As Figure 13, during the night (22 – 05 UTC).

5 Boundary layer properties

Figure 15 shows the seasonal cycle of the mean monthly diurnal temperature range (DTR) at 2 m above ground, defined as the difference between the average daily maximum and minimum temperatures. During winter and spring, there is a clear difference between relatively sheltered low-lying ground and exposed elevated terrain, with a 2 – 3°C higher DTR in valleys and over coastal plains. This is consistent with the empirical results obtained by Geerts (2003). Across the land area of Iceland, the lowest mean monthly values of DTR occur in October. This might be due to the fact that mean monthly relative humidity is highest during that month (not shown), together with significantly increased wind speeds compared with September and the summer months (see Figures 20 and 21 below). The highest mean monthly values of DTR occur in June in the northeast, such as around lake Mývatn.

The seasonal changes in relative heating and cooling between the land, the sea, and the atmosphere are clearly shown by the mean monthly temperature differences between the levels at 200 and 2 m above ground, in Figure 16 expressed as the vertical gradient per 100 m. Temperature at a fixed height of 200 m is calculated by linear interpolation between the fluctuating model levels. With the exception of the three summer months (JJA), the near-surface temperature gradient over land is predominantly positive, indicative of a very stable surface layer, with maximum values of about 2 K per 100 m during January in the northeast. Over the glaciers, vertical temperature gradients remain positive throughout the year. Over the ocean, on the other hand, they are predominantly negative, with the exception of the north and northeast coast during the summer months. This is due to negative sensible heat fluxes, driven by low sea surface temperatures, which were discussed in the previous section.

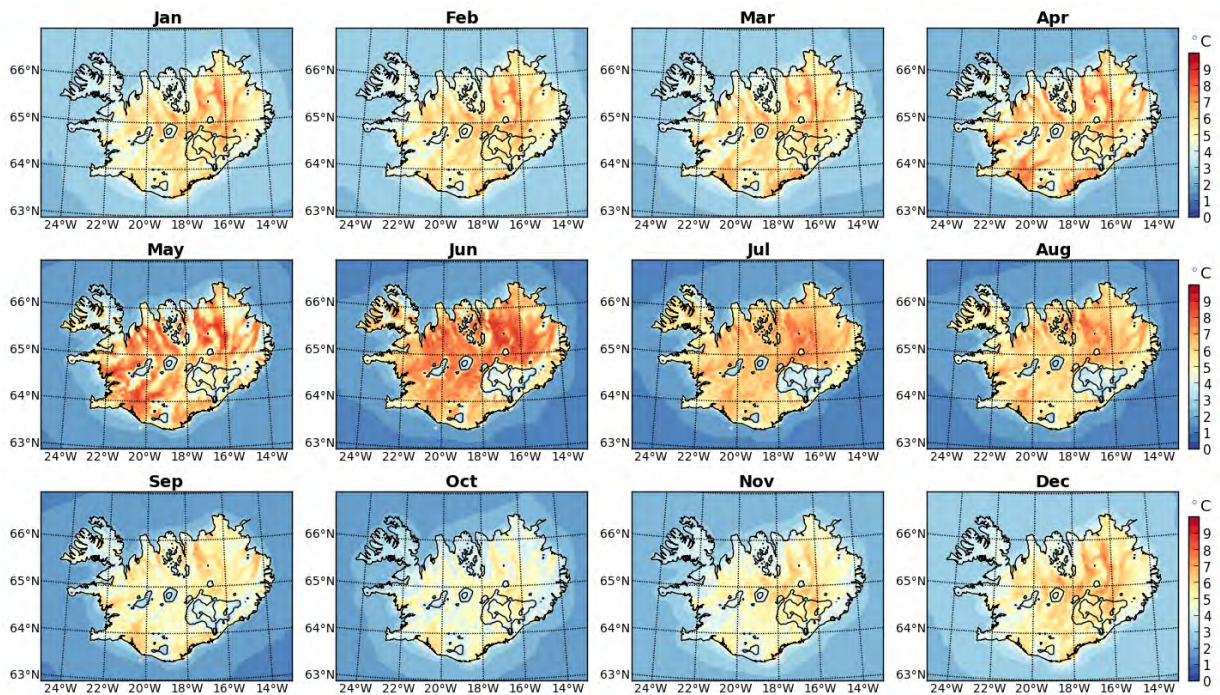


Figure 15. Mean monthly diurnal range of 2-m air temperature, defined as the difference between average daily maximum and minimum temperatures.

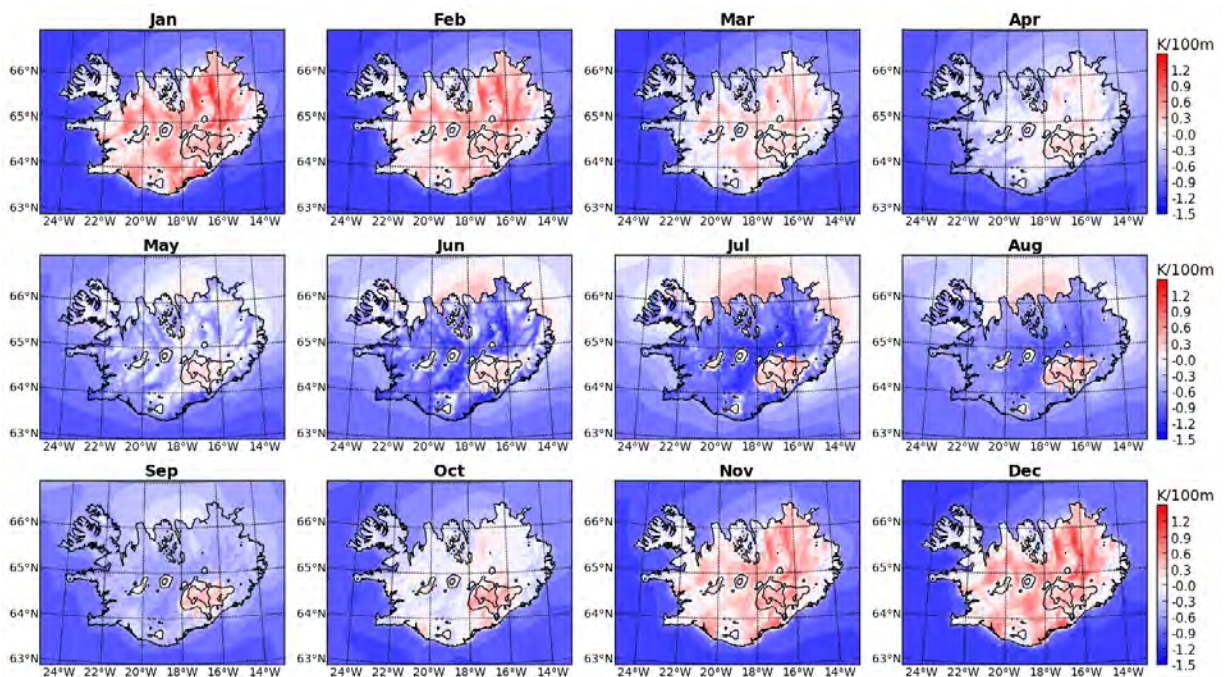


Figure 16. Mean monthly vertical temperature gradient within the layer between 2 and 200 m above ground.

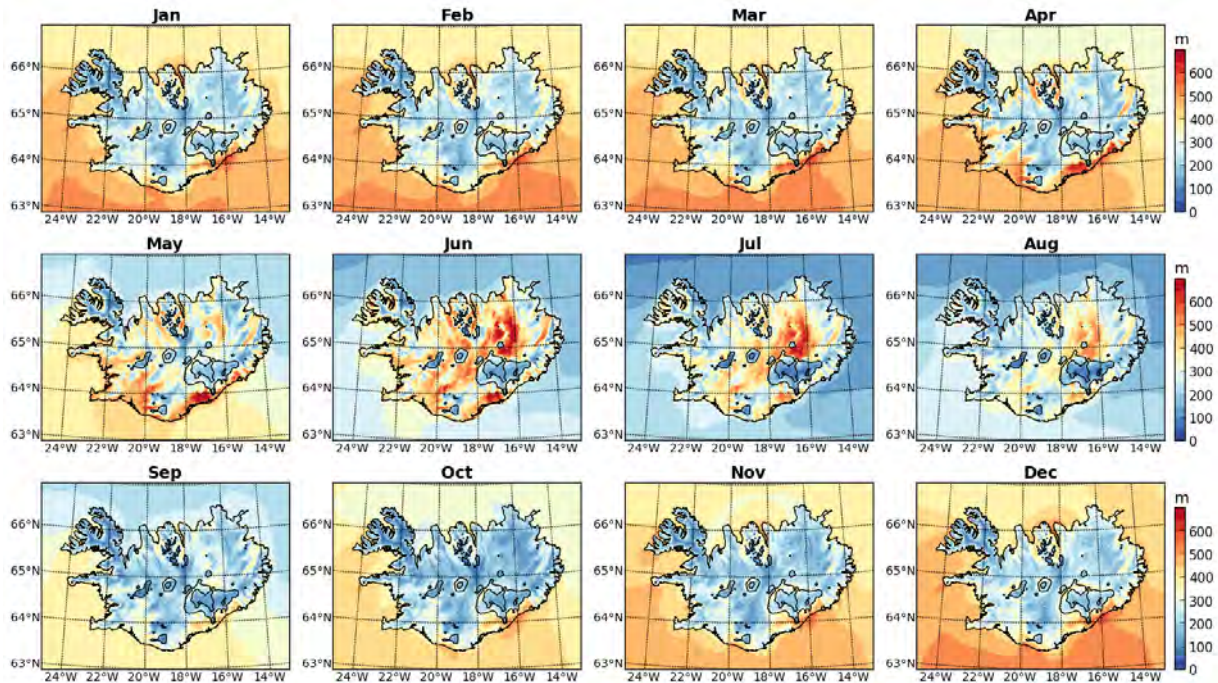


Figure 17. Mean monthly height of the lifted condensation level.

Figure 17 shows mean monthly fields of the lifted condensation level (LCL). According to Espy's equation, in units of metres above ground, it is estimated by $h_{lcl} = 125(T - T_d)$, with air temperature, T , and dew point temperature, T_d . Dew point temperature here is calculated from surface air pressure, 2-m temperature, and 2-m relative humidity. The LCL has well-defined and opposing seasonal cycles over the land and the ocean. Over land, it has the lowest monthly average in January, with values typically below 300 m. The highest monthly averages of 700 m occur in June over the rocky highlands north of Vatnajökull, as well as over the sandy region to the south of the glacier. Over the ocean, in contrast with the land, most of the incoming solar radiation in summer is converted to latent rather than sensible heat. Therefore, with increased evaporation and relative humidity, the average maritime LCL is lowest in July.

Two parameters of particular significance for agriculture and forestry are the number of frost days, as well as the accumulated growing degree days.

Frost days are defined here as those days with a minimum 2-m air temperature² below freezing. As shown in Figure 18, the only regions with an extended frost-free period from July through August are located southwest of the three main glaciers, as well as to the northwest of Langjökull. The coastal zone in the southwest has an additional month of frost-free period starting in June.

Following Björnsson et al. (2007b), growing degree days (GDD) are defined as the sum of positive deviations of daily mean 2-m temperatures from a threshold value of 5°C. As shown in Figure 19, based on air temperature, the growing season is primarily limited to the three summer months (JJA). At low elevations, the spatial variability of growing degree days matches quite

²Although air temperature directly above the ground is available as model output, these temperatures are likely to show the same or even larger negative biases as the values at 2 m above ground (see again Section 3). To avoid these unknown biases, recalculated 2-m temperatures are used here.

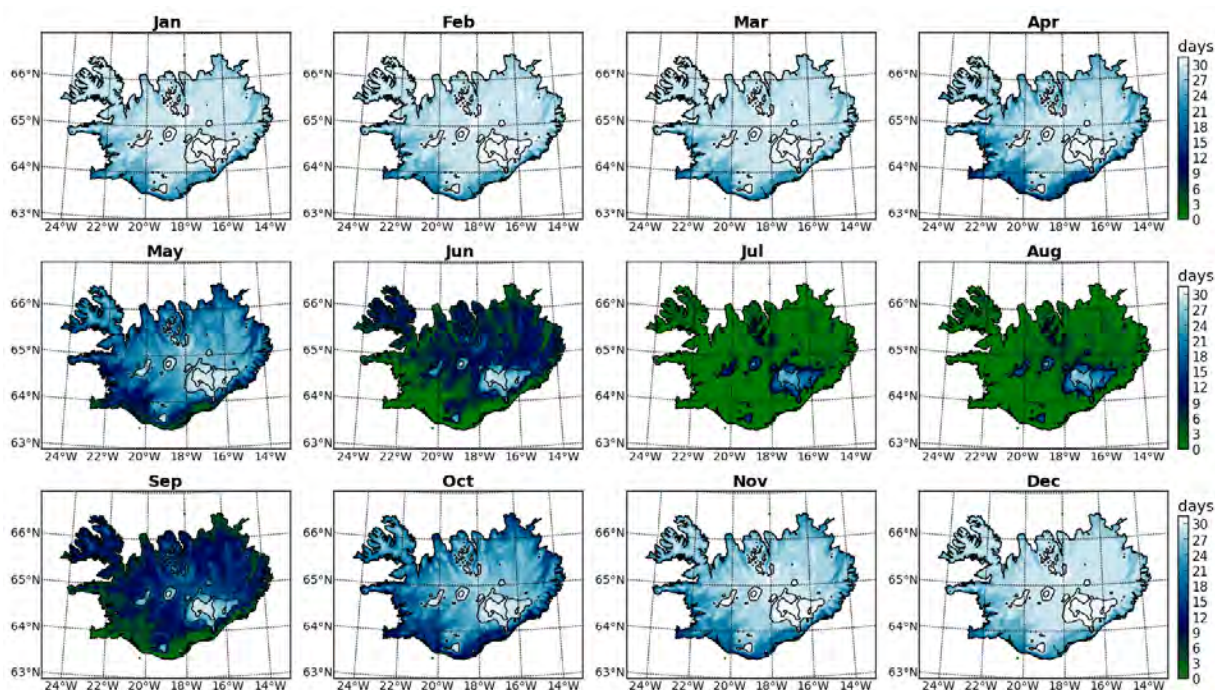


Figure 18. Number of frost days, with minimum 2-m air temperature below freezing. For a better comparison between different months, histograms are scaled to the same reference period of 30.5 days.

well the actual vegetation cover (see again Figure 1). Even in the coastal zone between Mýrdalsjökull and Vatnajökull, where the soil consists primarily of dark sand, the recent increase in the vegetation cover (Marteinsdóttir et al., 2007) may be supported, at least in part, by the high number of GDD in that region. Over the interior highlands, plant growth is limited not only by soil type, but also by a reduced growth and extended frost period. The annual accumulation of simulated growing degree days matches well the results obtained by Bjornsson et al. (2007b), based on spatially interpolated and bias corrected station measurements for the 1961 – 90 period (see Bjornsson et al. (2007) for the calculation of monthly temperature fields). The largest differences are found in the coastal zone between Mýrdalsjökull and Vatnajökull, with around 600 GDD per year according to the interpolated measurements, and around 750 GDD according to the reanalysis. This is despite the fact that monthly averages of 2-m air temperature in that region are consistent.

Figures 20 and 21 show the seasonal cycle of the prevailing 10-m wind conditions during the day and the night, respectively. As in the previous section, daytime hours are defined as the 10 – 17 UTC period, and nighttime hours as the 22 – 05 UTC period. The wind vectors shown in these figures are composites of average wind speed and the direction of the average unit wind vector. They are therefore not representative of the net flow, which would be given by the average horizontal wind vector. From October through April, the prevailing wind field within the model domain is determined by the combination of strong northeasterly winds along the southeast coast of Greenland (itself outside the computational domain) with the cyclonic circulation in the southwest such that Iceland is immersed in a predominantly southeasterly to easterly flow. During that period, the difference between day- and nighttime prevailing winds is small and

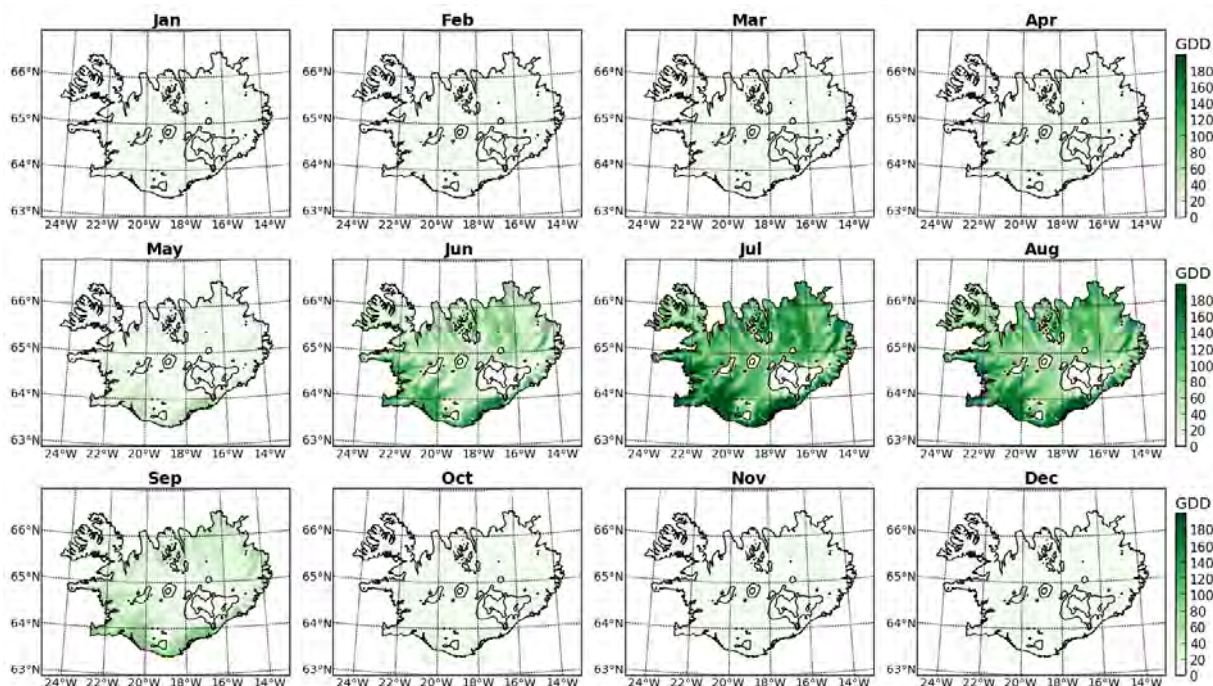


Figure 19. Monthly growing degree days (GDD, see main text for definition).

unsystematic. Throughout the day, the thermal differences between the land area and the surrounding ocean generate downslope and offshore winds that, along the southeast and east coast, are directed against the maritime winds. During the remaining part of the year, May through September, the winds over the ocean weaken, and temperature-driven diurnal fluctuations in the low-level wind field over land become more important. The main changes over the course of the day occur along the south coast, where onshore winds intensify from around 3.5 m s^{-1} during the night to around 6.5 m s^{-1} during the day. Despite that, due to katabatic forcing, low-level winds around Vatnajökull remain predominantly divergent.

The significance of thermal forcing for low-level winds in summer can easily be seen by analysing the mean monthly vertical gradient in wind speed within the layer between 10 and 200 m above ground (see Figure 22). Despite the fact that surface roughness increases in summer, as the extent of snow cover decreases, and the height and density of vegetation increases, the vertical wind speed gradient is significantly reduced compared with the winter months, especially over the near-coastal ocean, where sea breezes are generated by the differential heating of land and water surfaces.

The mean monthly wind power density at 50 m above ground is shown in Figure 23, where power density is given by $0.5 \rho v^3$, with air density ρ , and wind speed v . These results are consistent with those derived from corrected WRF model data for the 1995 – 2008 period, which was discussed by Nawri et al. (2013) and Nawri et al. (2014). The conclusions of these earlier publications about the commercial viability of wind power production in Iceland are therefore confirmed by the more recent model simulations.

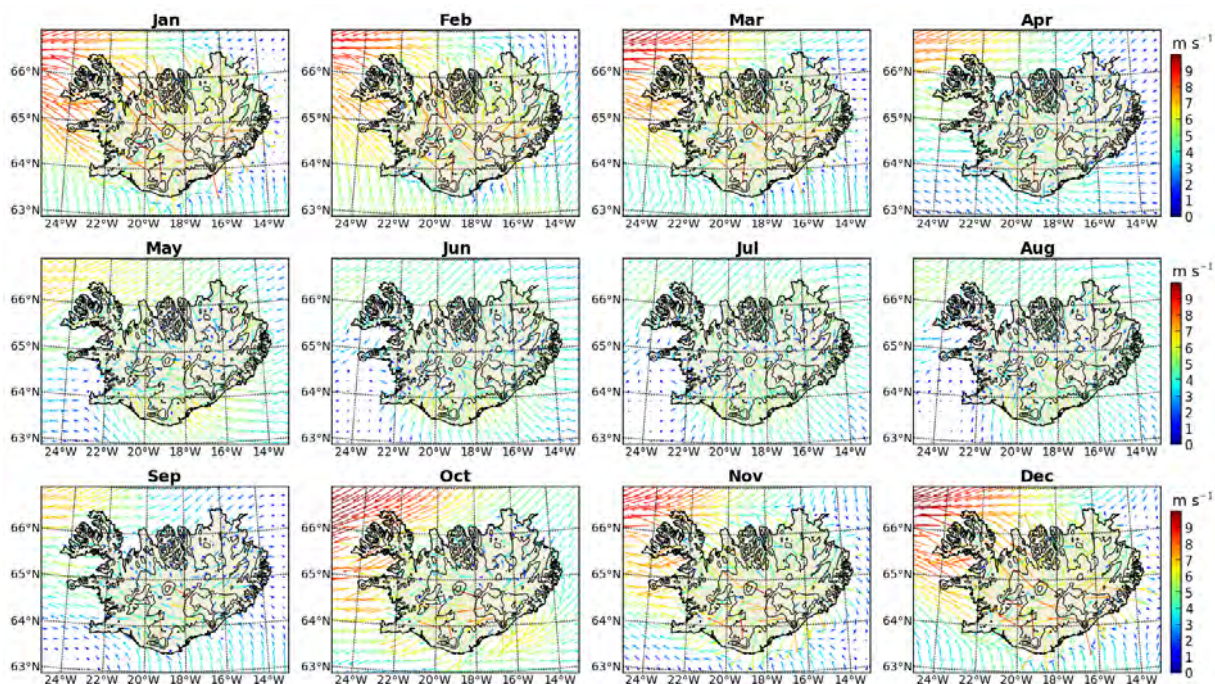


Figure 20. Prevailing 10-m wind conditions during the day (10 – 17 UTC). Wind vectors are composites of average wind speed and the direction of the average unit wind vector.

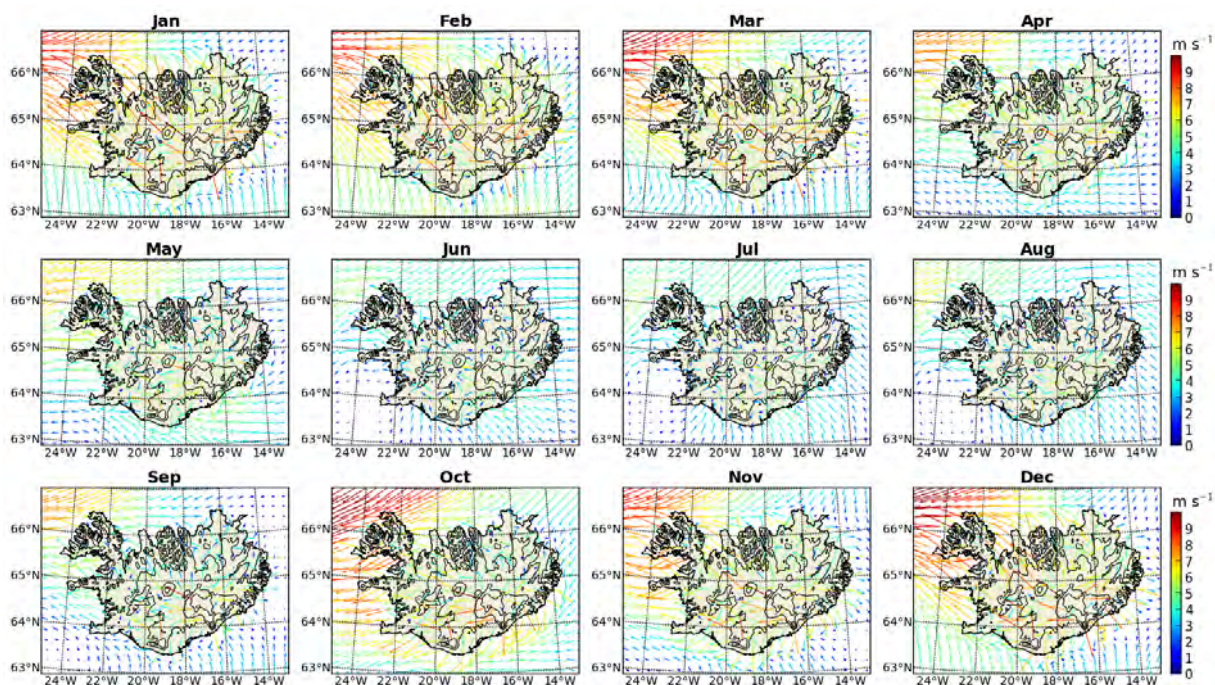


Figure 21. As Figure 20, during the night (22 – 05 UTC).

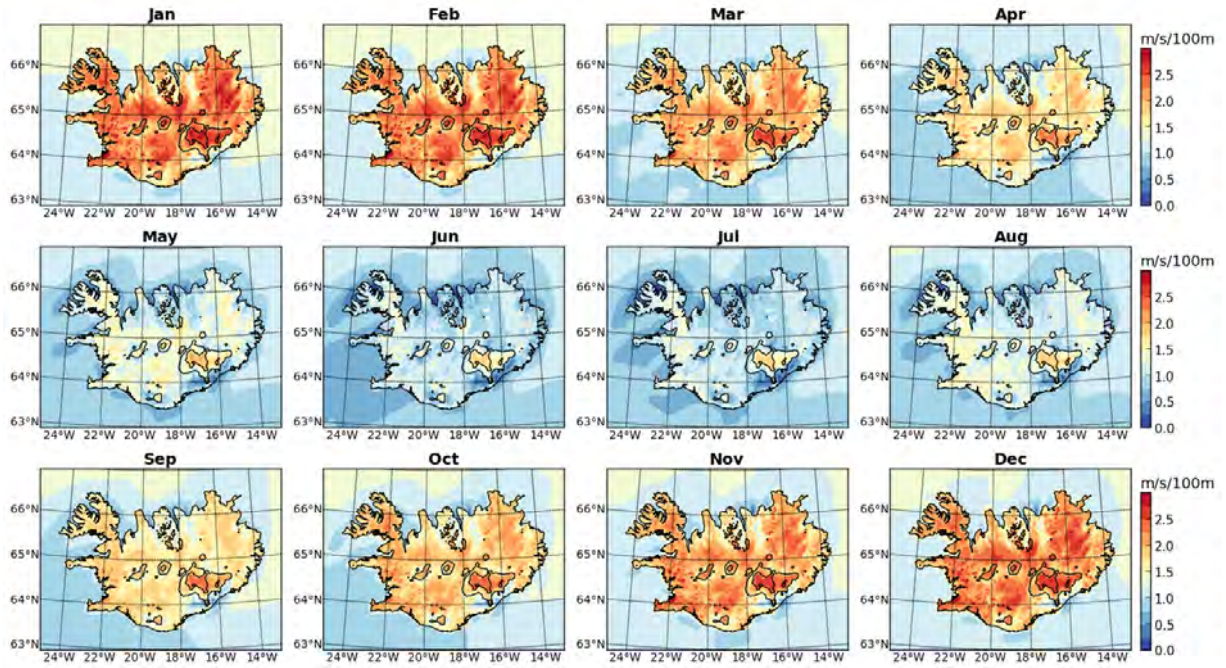


Figure 22. Mean monthly vertical gradient of wind speed within the layer between 10 and 200 m above ground.

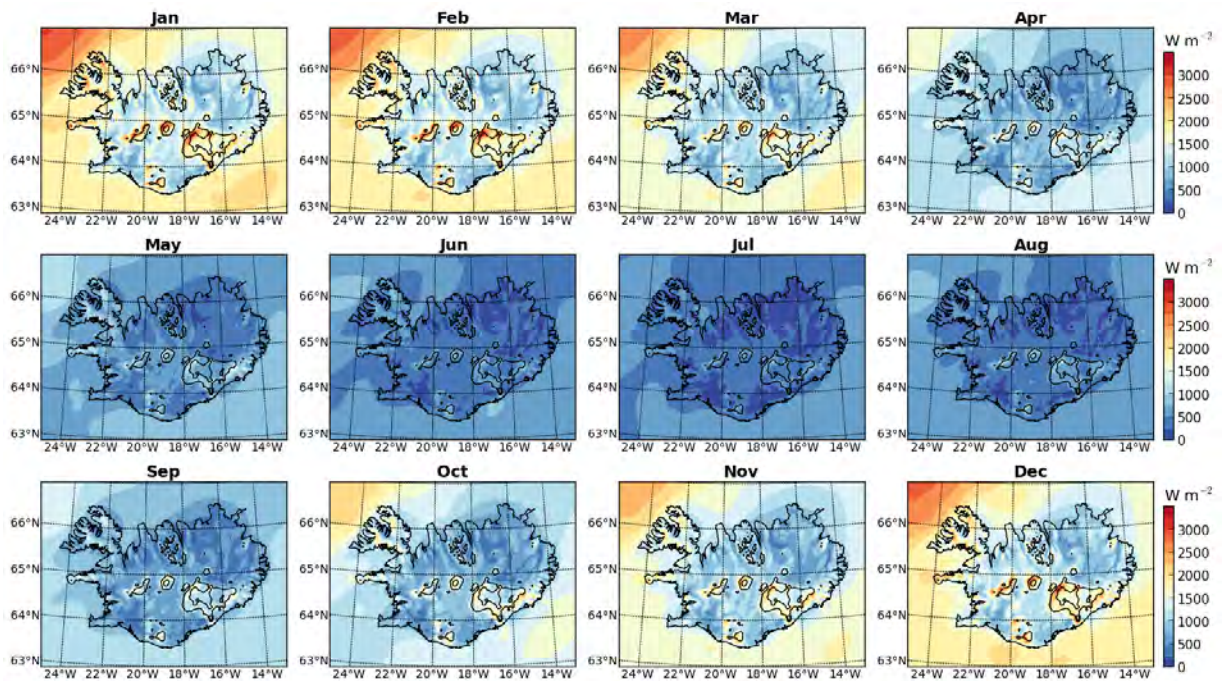


Figure 23. Mean monthly wind power density at 50 m above ground.

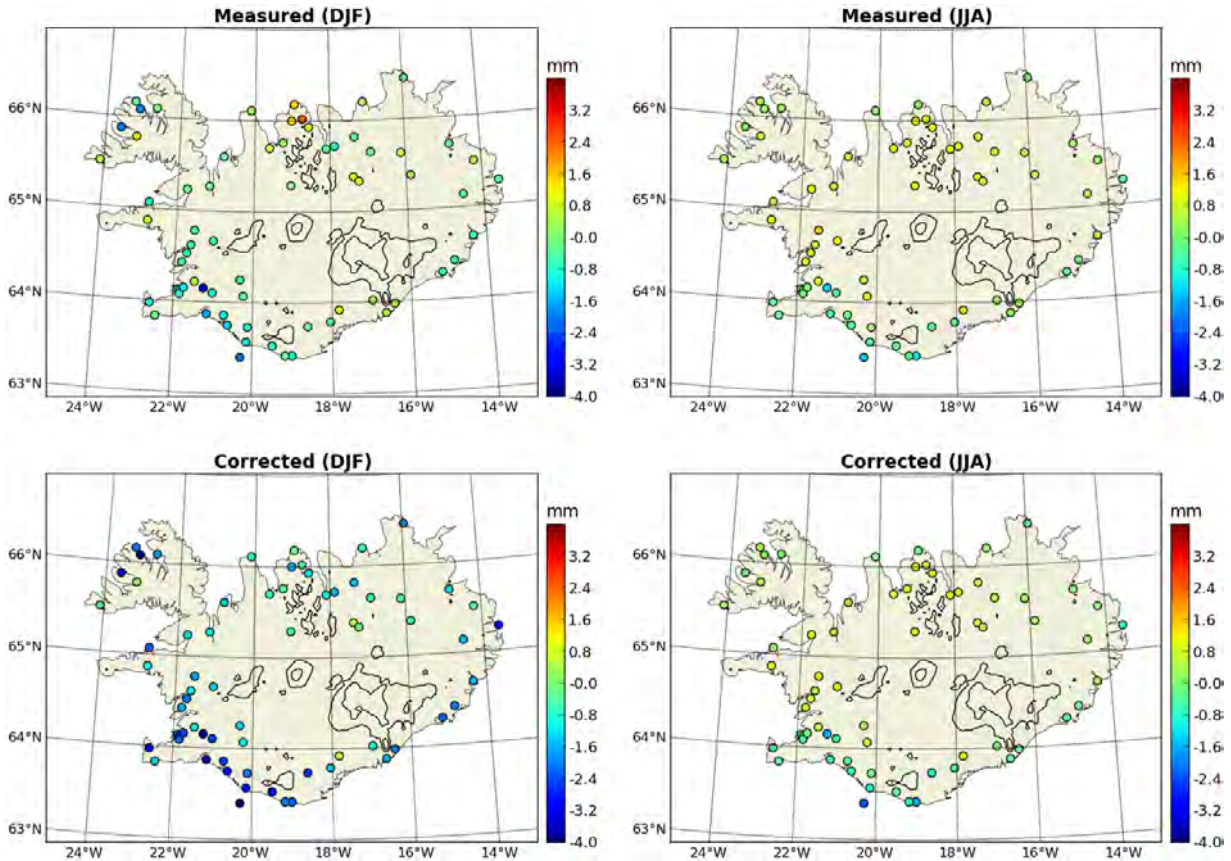


Figure 24. Simulated daily precipitation biases relative to original and wind-loss corrected gauge measurements in winter (DJF) and summer (JJA).

6 Precipitation

In validation studies conducted at IMO, it has been shown that total precipitation from HARMONIE-AROME simulations provides a closer match with gauge measurements than a linear model of orographic precipitation that had previously been used in climatological studies (for a description of the linear model see Crochet et al. (2007) and Crochet (2012)). However, a comparison with quality controlled gauge measurements for the period 1991 – 2011, with 24-hour amounts accumulated from 09 UTC on the previous day, shows that there are systematic biases in simulated precipitation, especially in winter. Comparisons were made with both the original measurements, as well as with the wind-loss corrected (increased) values. Even compared with the original measurements, model biases are predominantly negative along the south coast, and either less negative or slightly positive over the northern part of the country (see Figure 24). Over the complex terrain of the Westfjords, simulated precipitation shows a large spatial variability, with positive and negative biases in winter, but a close match with measured values in summer. Compared with wind-loss corrected measurements, biases are consistently negative in winter. In summer, with the exception of the south coast, precipitation biases relative to corrected values are small. Notwithstanding these overall negative biases, throughout most of the country, the model overestimates daily precipitation more often than underestimating it (see Figure 25). With the exception of the western coastal regions, in comparison with wind-loss corrected measurements in winter, the prevailing negative biases are therefore predominantly due to the underestimation of a few extreme events.

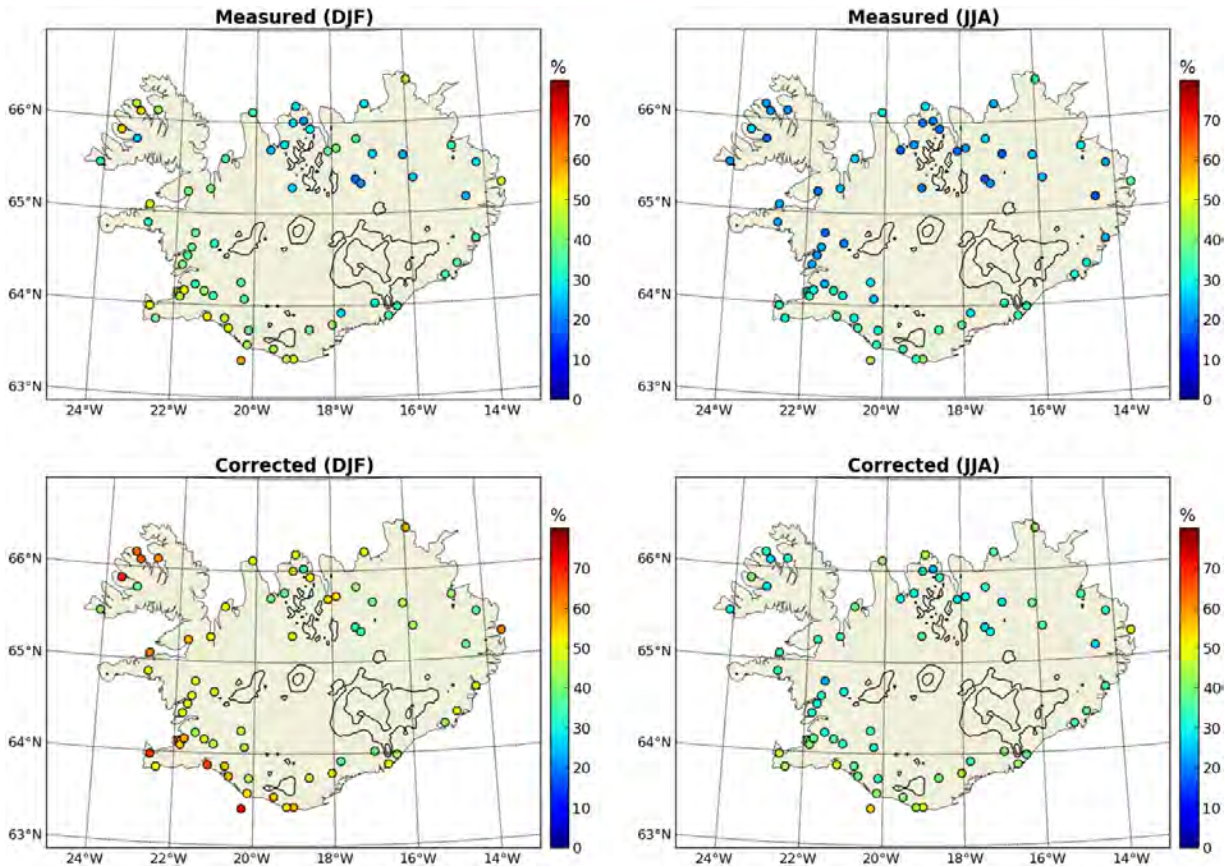


Figure 25. Percentage number of days during which simulated daily precipitation was less than the originally measured and wind-loss corrected accumulation in winter (DJF) and summer (JJA).

As shown in Figure 26, the simulated mean monthly total accumulation of precipitation – including rain, snow, and mixed-phase – has a well-defined seasonal cycle, with the lowest (highest) amounts in June (December). However, greater than the seasonal differences is spatial variability, with the highest precipitation amounts occurring on slopes facing the prevailing winds (refer again to Figure 21), especially along the southeast coast.

Net precipitation received by the ground is given by the difference between total precipitation and the sum of evaporation and sublimation. During the summer (JJA), the daytime (10 – 17 UTC) accumulation of total precipitation exceeds the nighttime (22 – 05 UTC) accumulation by between 10 – 40 mm within each month over the Icelandic land area (not shown). At the same time, however, the accumulated daytime evaporation from snow-free ground exceeds nighttime evaporation by 30 – 60 mm. As shown in Figure 27, this results in a daytime net accumulation of precipitation that is reduced by up to 50 mm within each month relative to the nighttime net accumulation. In winter, the diurnal cycle in solar forcing and related atmospheric processes over Iceland is weak, and precipitation is primarily driven by large-scale circulation features.

There is a well-defined seasonal change in the typical duration of precipitation events, with individual events defined here as being separated by at least one hour at each grid point. As shown in Figure 28, precipitation events that last up to 6 hours are most frequent in July and August. By

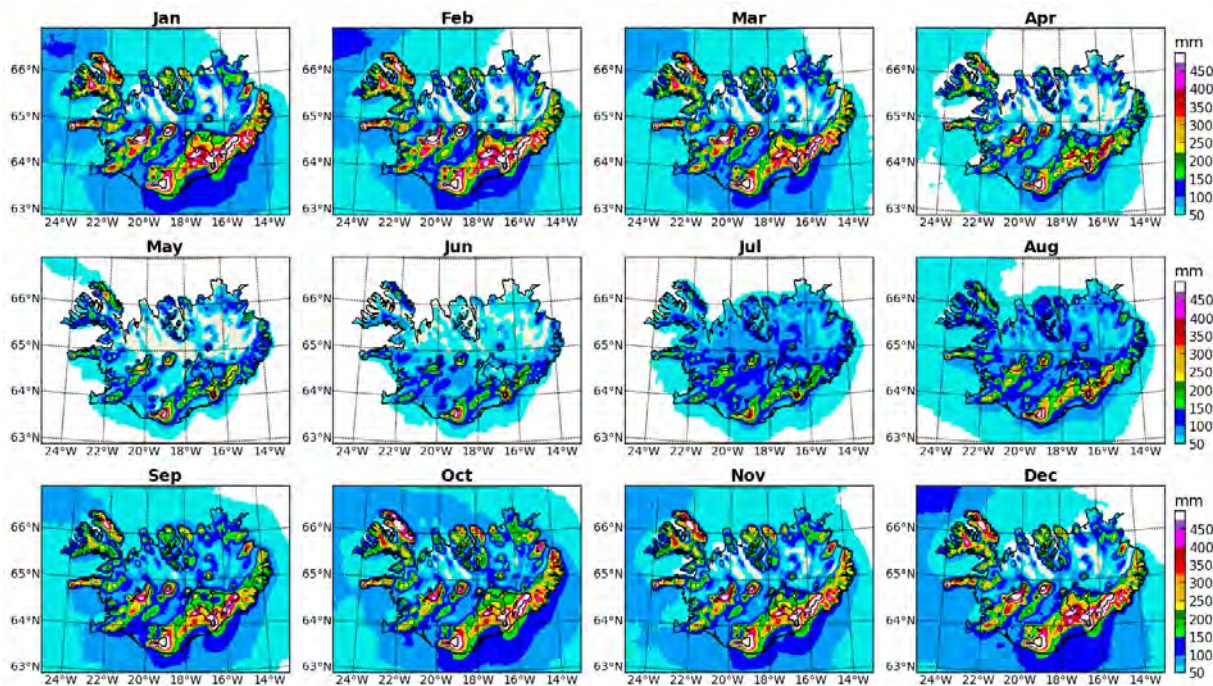


Figure 26. Accumulation of total precipitation, including rain, snow, and mixed-phase. For a better comparison between different months, accumulations are scaled to the same reference period of 30.5 days.

contrast, precipitation events lasting more than 6 and up to 12 hours are most frequent between December and March (see Figure 29), the same being true for precipitation events lasting more than 12 hours (not shown). This is indicative of a shift between winter and summer in the relative occurrence of stratiform precipitation related to cyclonic activity, and more localised convective precipitation.

The intensity (total accumulation) of precipitation events with similar durations also shows a clear seasonal shift, with the highest average intensities occurring along the coast in winter (DJF), and in the interior in summer, particularly in July. For precipitation events lasting up to 6 hours, this is shown in Figure 30, but qualitatively the same patterns are found for longer events. This geographical shift in precipitation intensity is consistent with the summertime increase in convection and evaporation (sensible and latent heat fluxes) over the land area (see again Section 4).

As shown in Figure 31, the spatial distribution of heavy precipitation events with accumulations between 16 – 30 mm is closely tied to the orography. They occur most frequently during the winter months along south- or southeast-facing slopes, particularly along the southeast coast, where prevailing onshore winds are forced to ascend. The more convective summertime precipitation events tend to last shorter and have lower total accumulation amounts.

Information about the absorption of water by the ground is not available as model output. It is therefore impossible to determine runoff accurately. However, an upper limit, or potential runoff, can be estimated by calculating the amount of liquid water added to the surface. During

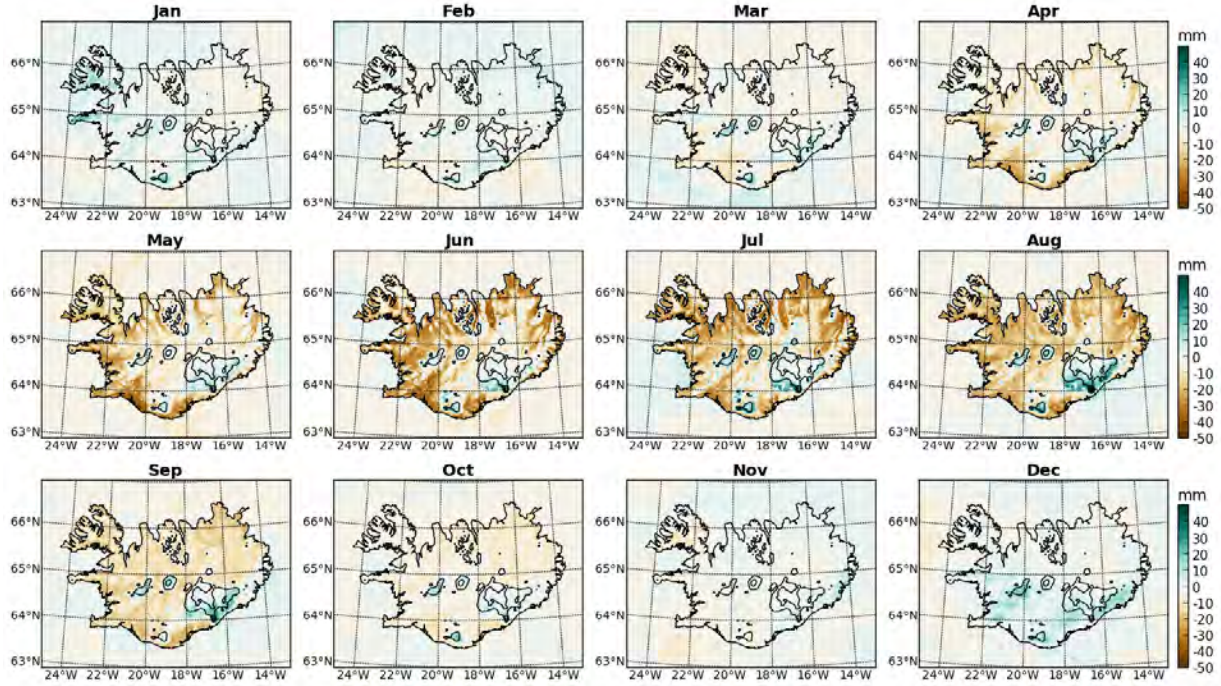


Figure 27. Difference in net precipitation (as liquid water equivalent) between daytime (10 – 17 UTC) and nighttime (22 – 05 UTC) hours. For a better comparison between different months, accumulations are scaled to the same reference period of 30.5 days.

a particular hour, t , it is given by

$$W_t = R_t - E_t + M_t , \quad (1)$$

where R_t is the hourly rain rate, E_t is hourly evaporation, and M_t is hourly snowmelt, which is given by the difference between potential and actual snow depth (measured as liquid water equivalents) at the beginning of the following hour,

$$M_t = D_{pot,t+1} - D_{t+1} . \quad (2)$$

Potential snow depth is calculated by adding the accumulated solid precipitation (snow and graupel) that fell during that hour to the actual snow depth at the beginning of the hour, and by subtracting hourly sublimation,

$$D_{pot,t+1} = D_t + S_t + G_t - Su_t . \quad (3)$$

More explicitly, (1) can then be written as the total net precipitation, minus the forward-in-time differential of the liquid water equivalent of snow cover on the ground,

$$W_t = R_t + S_t + G_t - E_t - Su_t - (D_{t+1} - D_t) . \quad (4)$$

Mean monthly fields of potential runoff, calculated in that fashion, are shown in Figure 32. From October through April, it is primarily determined by rainfall, and highest in a narrow band along the southeast coast. Starting in May, with the widespread onset of snowmelt, potential runoff exceeds monthly rainfall by more than a factor of two, even along the southeast coast. Until the end of September, it is then determined primarily by the melting of the seasonal snow cover.

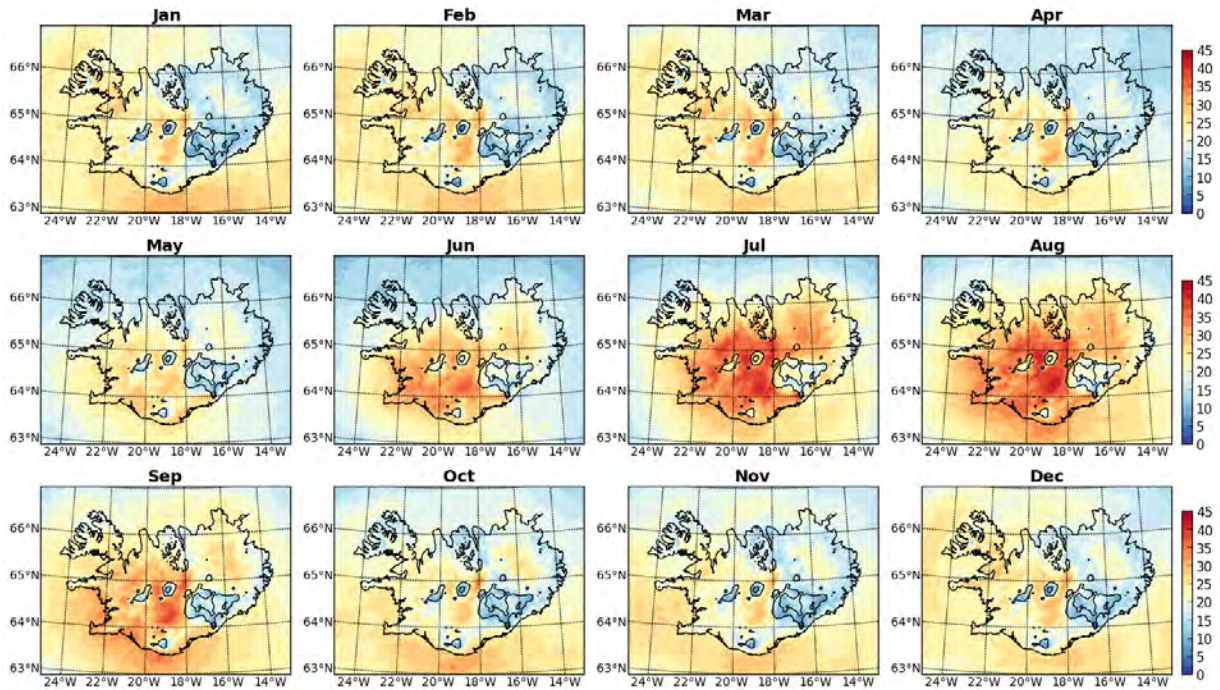


Figure 28. Occurrence of precipitation events lasting up to 6 hours. For a better comparison between different months, occurrences are scaled to the same reference period of 30.5 days.

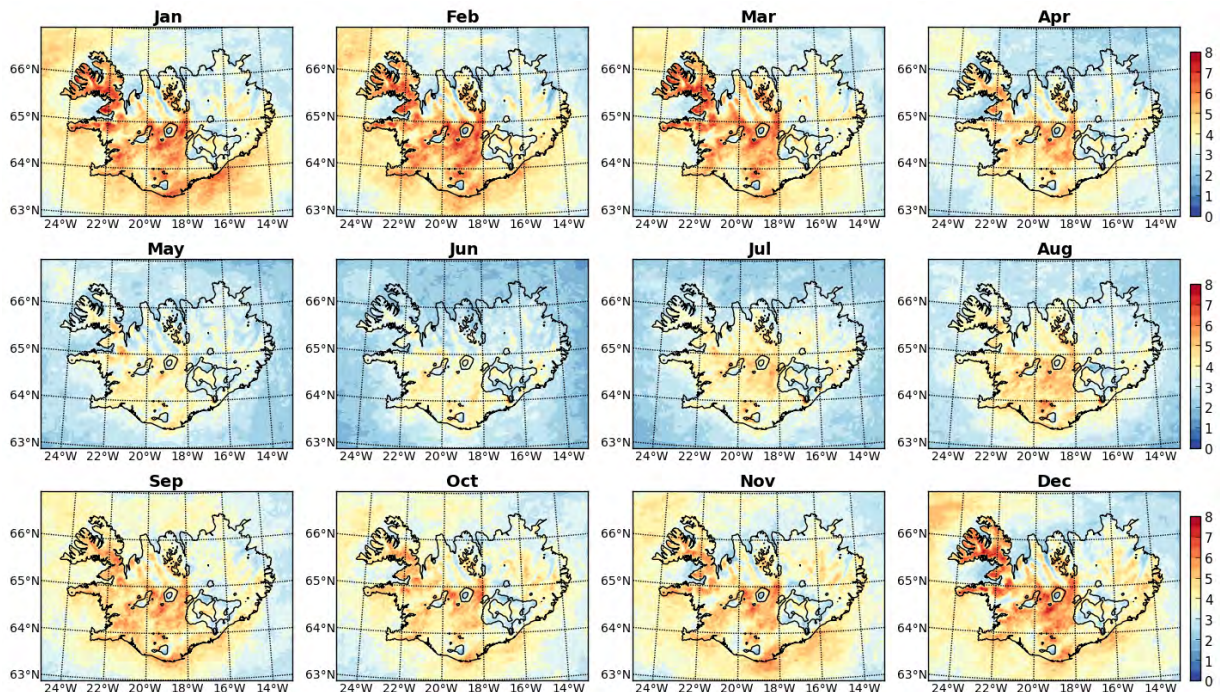


Figure 29. Occurrence of precipitation events lasting more than 6 and up to 12 hours. For a better comparison between different months, occurrences are scaled to the same reference period of 30.5 days.

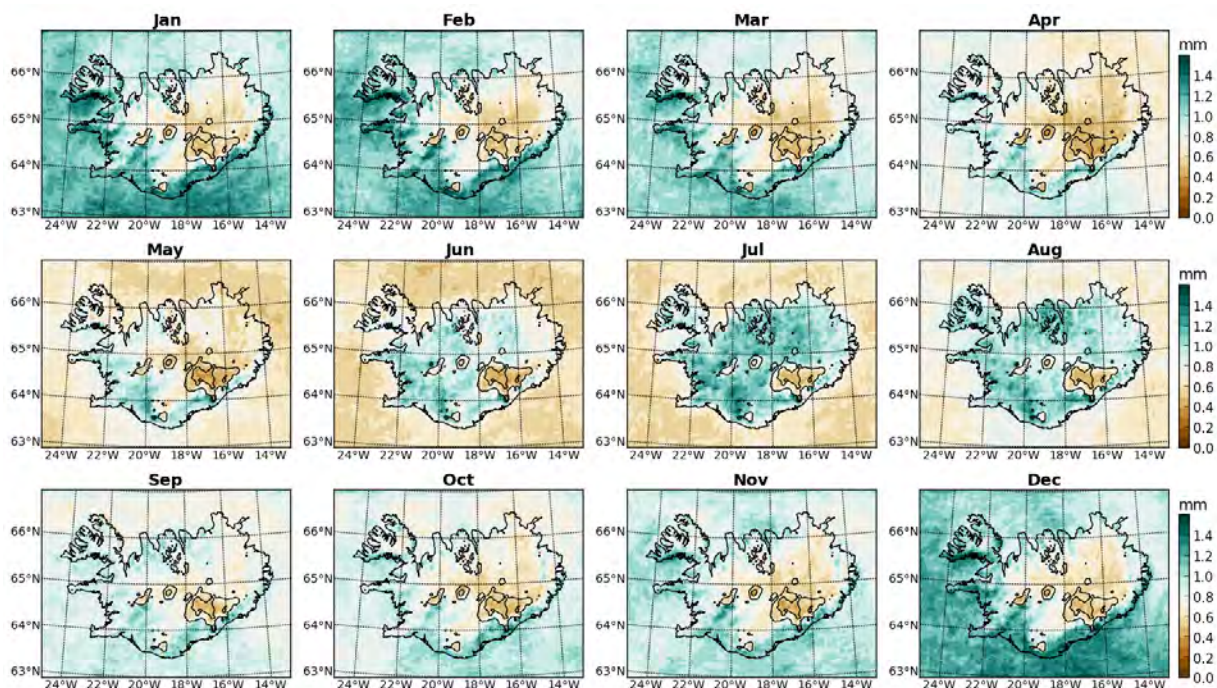


Figure 30. Average intensity (total accumulation as liquid water equivalent) of precipitation events lasting up to 6 hours.

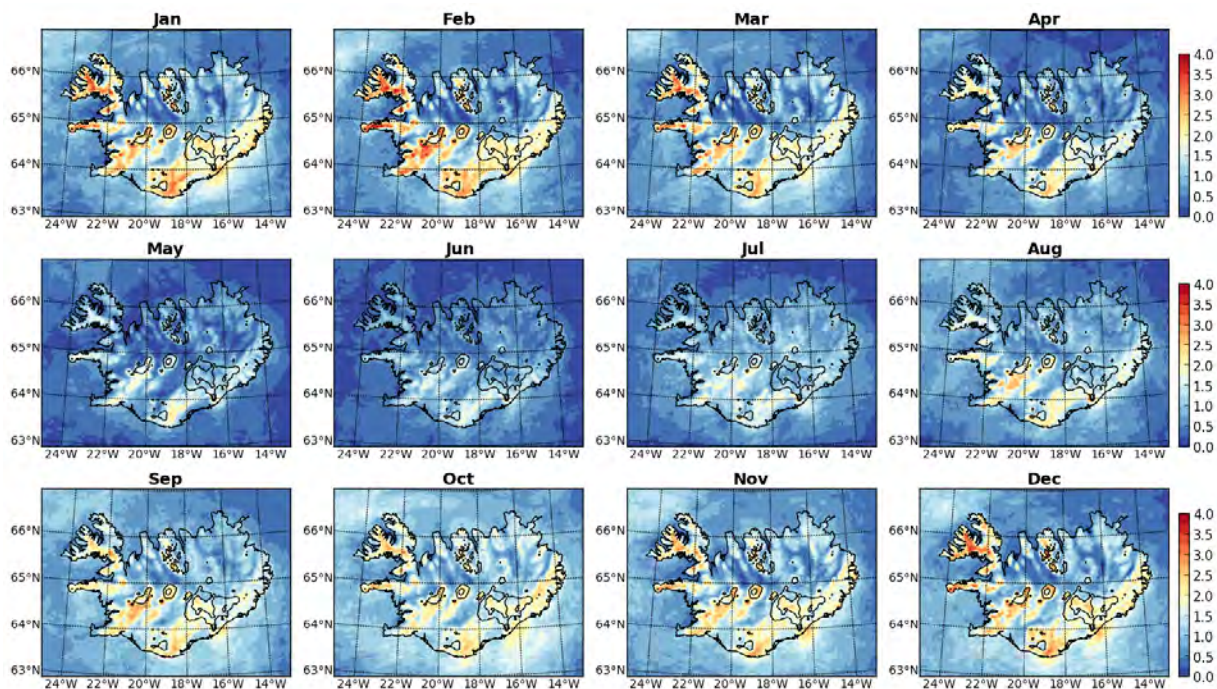


Figure 31. Occurrence of precipitation events with total accumulation as liquid water equivalent of more than 15 and up to 30 mm. For a better comparison between different months, occurrences are scaled to the same reference period of 30.5 days.

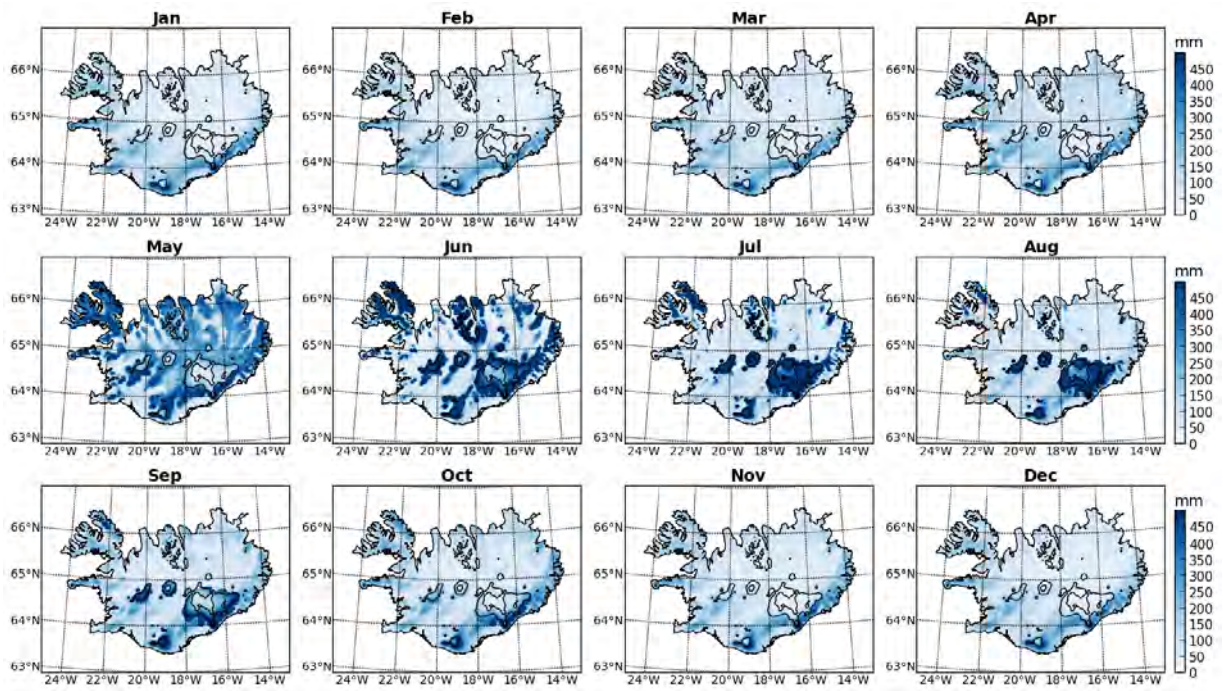


Figure 32. Mean monthly accumulation of liquid water on the ground (potential runoff) from net rainfall and snowmelt.

7 Conclusions

This report describes the ICRA reanalysis project for Iceland, which was initiated by the Icelandic Meteorological Office in the autumn of 2015, using the HARMONIE-AROME mesoscale numerical weather prediction model. The objective here was not to provide a comprehensive climatology, but rather to serve as a technical reference for future scientific studies based on the reanalysis data.

For the first time, the reanalysis allows the calculation of the surface energy balance over the entire land area of Iceland, establishing the relative importance of radiation and heat fluxes, their spatial variability, and changes on diurnal and seasonal time-scales. The results demonstrate that the model reacts to geographical differences and to the solar cycle in a manner that is qualitatively plausible and internally consistent.

It was then shown how the temporal and spatial variability of energy fluxes is consistently related to the variability of different boundary layer properties, such as the diurnal temperature range, diurnal shifts in the horizontal wind field, and the vertical gradients of temperature and wind speed.

Furthermore, a number of statistics, derived from hourly grid-point time-series, were discussed. They give an insight into the frequency of occurrence of certain weather events, such as frost and growth days, or of precipitation events with specific durations and intensities. These were also shown to be systematically linked to seasonal changes and geographical differences.

Finally, the high level of wind power density over Iceland, that had been determined in previous studies based on a different mesoscale model dataset, was confirmed by the reanalysis data.

As a numerical dataset describing the atmospheric boundary layer over Iceland, ICRA is unprecedented in its scope, providing possibilities for a wide range of applications from, e.g., wind energy assessments to dispersion and hydrological studies.

References

- Andersson, E., & Thépaut, J. N. (2008). ECMWF's 4D-Var data assimilation system – the genesis and ten years in operations. *ECMWF Newsletter*, 115, 8-12.
- Bechtold, P., Köhler, M., Jung, T., Doblas-Reyes, F., Leutbecher, M., Rodwell, M. J., ... Balsamo, G. (2008). Advances in simulating atmospheric variability with the ECMWF model: from synoptic to decadal time-scales. *Q. J. R. Meteorol. Soc.*, 134, 1337-1351.
- Bengtsson, L., Andrae, U., Aspelien, T., Batrak, Y., Calvo, J., de Rooy, W., ... Køltzow, M. Ø. (2017). The HARMONIE-AROME model configuration in the ALADIN-HIRLAM NWP system. *Mon. Wea. Rev.*, 145, 1919-1935.
- Bjornsson, H., Jonsson, T., Gylfadottir, S. S., & Olason, E. O. (2007). Mapping the annual cycle of temperature in Iceland. *Meteorol. Z.*, 16(1), 45-56.
- Bjornsson, H., Olason, E. O., Jónsson, T., & Henriksen, S. (2007b). Analysis of a smooth seasonal cycle with daily resolution and degree day maps for Iceland. *Meteorol. Z.*, 16(1), 57-69.
- Brousseau, P., Berre, L., Bouttier, F., & Desroziers, G. (2011). Background-error covariances for a convective-scale data-assimilation system: AROME – France 3D-Var. *Q. J. R. Meteorol.*

- Soc.*, 137, 409-422.
- Crochet, P. (2012). *High resolution precipitation mapping in Iceland by dynamical downscaling of ERA-40 with a linear model of orographic precipitation* (Report VÍ 2012-003). Reykjavik, Iceland: Icelandic Meteorological Office.
- Crochet, P., Jóhannesson, T., Jónsson, T., Sigurðsson, O., Björnsson, H., Pálsson, F., & Barstad, I. (2007). Estimating the spatial distribution of precipitation in Iceland using a linear model of orographic precipitation. *J. of Hydrometeorol.*, 8(6), 1285-1306.
- Geerts, B. (2003). Empirical estimation of the monthly-mean daily temperature range. *Theor. Appl. Climatol.*, 74, 145-165.
- Hanna, E., Jónsson, T., Ólafsson, J., & Valdimarsson, H. (2006). Icelandic coastal sea surface temperature records constructed: Putting the pulse on air-sea-climate interactions in the northern North Atlantic. Part I: Comparison with HadISST1 open-ocean surface temperatures and preliminary analysis of long-term patterns and anomalies of SSTs around Iceland. *J. Climate*, 19, 5652-5666.
- Le Moigne, P. (2009). *SURFEX scientific documentation*. Toulouse, France: CNRM.
- Marteinsdóttir, B., Svavarsdóttir, K., & Þórhallsdóttir, Þ. E. (2007). Landnám birkis á Skeiðarásandi. *Náttúrufræðingurinn*, 75(2-4), 123-129.
- Nawri, N. (2014). *Evaluation of HARMONIE reanalyses of surface air temperature and wind speed over Iceland* (Report VÍ 2014-005). Reykjavik, Iceland: Icelandic Meteorological Office.
- Nawri, N., Petersen, G. N., Björnsson, H., Hahmann, A. N., Jónasson, K., Hasager, C. B., & Clausen, N.-E. (2014). The wind energy potential of Iceland. *Renewable Energy*, 69, 290-299.
- Nawri, N., Petersen, G. N., Björnsson, H., & Jónasson, K. (2013). *The wind energy potential of Iceland* (Report VÍ 2013-001). Reykjavik, Iceland: Icelandic Meteorological Office.
- Palmason, B., Thorsteinsson, S., Nawri, N., Petersen, G. N., & Björnsson, H. (2016). HARMONIE activities at IMO in 2015. *ALADIN-HIRLAM Newsletter*, 6, 72-75.
- Seity, Y., Brousseau, P., Malardel, S., Hello, G., Bénard, P., Bouttier, F., ... Masson, V. (2011). The AROME-France convective-scale operational model. *Mon. Wea. Rev.*, 139, 976-991.
- WMO. (2012). *Guide to meteorological instruments and methods of observation*, WMO-No. 8, 7th edition, updated in 2010 and 2012. Geneva, Switzerland: World Meteorological Organization.